Universiteit Utrecht

Faculty of Geosciences

Flow Separation in Sharp-Bend-Flow

M.Sc. thesis

Utrecht 2014

Author: *Ruben Ardesch*

Student nr.: *3860892*

M.Sc. program: *Earth, Surface & Water*
M.Sc. track: *Coastal Dynamics & Fluvial Systems*

Supervisor: *dr. M. Kleinhans*

Second supervisor: *prof. dr. D. Parsons*

Second corrector: *dr. M. van der Vegt*

Preface

This thesis was written as the penultimate work of the Master programme of Earth, Surface & Water. The goal of this thesis was to demonstrate my level of academic skill and my knowledge and understanding of coastal dynamics and fluvial systems. Due to health problems the writing of this thesis has taken up more time than desirable, however I hope that the time was well spent and I have delivered work of good quality. If this thesis is of sufficient quality, I will be awarded with 37.5 ECTS.

Abstract

In sharp-bend-flow the hydrodynamic phenomena are different than in straight channel flow. Flow separation and hdelical flow are the most important sharp-bend-flow phenomena and they have a major morphological effect. Literature states that the transverse water surface tilt is an important factor in determining the internal processes of flow separation and helical flow and that flow depth and roughness influence the transverse tilt. Literature also states that the effects of flow separation are flow recirculation, contraction of the main flow, a shear layer, shear layer-induced vorticity, interaction between hydraulic phenomena and separation-sediment interaction. The exact causes and internal processes of flow separation remain unknown. Experimental laboratory data-sets of surface flow structures were analyzed and several maps were made to try to fill the knowledge gap.

The results showed that an increase in flow depth and/or Froude number both lead to an increase in transverse water level tilt, thus promoting helical flow and flow separation by creating an adverse pressure gradients. The flow separation creates a sharp transition in flow velocity that starts halfway the inner bend and diffuses downstream while creating vorticity. Flow recirculation was not significant in the constant width bend, but outer bank widening was likely the cause of considerable flow recirculation. The larger the flow depth the smaller the extent of the recirculation zone. The shear layer “flaps” with a period of approximately 13 seconds over 6% of the flow width. An increase in flow depth resulted in a downstream movement of the shear layer and an increase in the Froude number caused the downstream end of shear layer to bend towards the inner bend.

Table of contentss

List of figures

List of tables

1 Introduction

When taking shelter from a storm, just behind the edge of a building, the fast moving air passes by and is not able to blow you away. The reason of the relative calm air, is that the wind is not able to redirect itself quickly enough to make the sharp turn. The wind separates from the wall of the building and takes a more gentle turn, resulting in a region of slow moving air downstream of the edge. Figure 1 is a flow visualization that shows flow separation that resembles the situation mentioned above. The fast moving fluid does not follow the wall downstream of the sharp edge, this creates a sharp transition in flow velocity, also called shear layer. The sharp transition in flow velocity is the definition of flow separation.

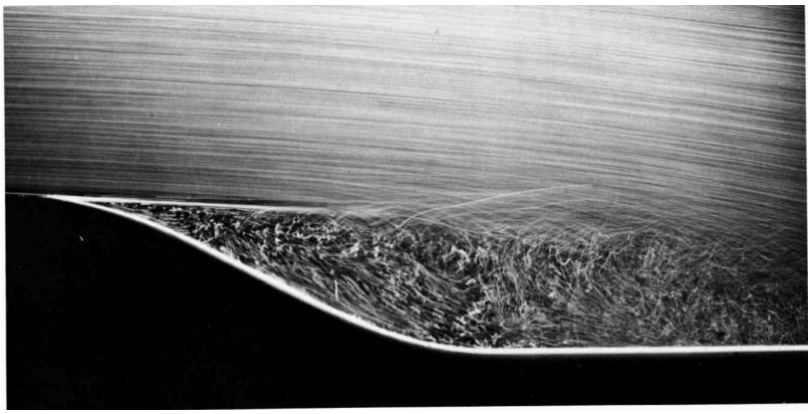

Figure 1, Turbulent flow separation from laminar flow past a curved wall (Van Dyke, 1982)

Another example is the wing of an airplane (Figure 2), normally the air flows “smoothly” over the wing with a thin viscosity-induced boundary layer. When the angle of incidence is increased to a specific value the flow over the wing separates, increasing the extent of the boundary layer.

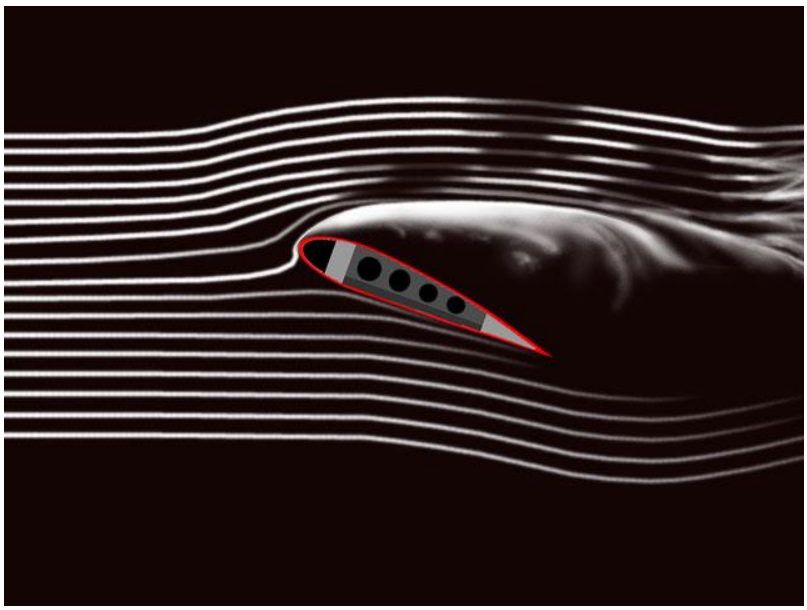

Figure 2, Flow separation over an airfoil (Franklin Institute, 1999)

The same phenomenon takes place in water. For example in rivers where sharp edges are present, such as: sharp river bends, engineered structures, bedforms and river channel bifurcations. It should be noted that in rivers there is an outer- and inner-bank that contains the flowing water, so the water

is forced to follow the bend. This results in more complex situations than wind passing a building or a wing moving through air.

Flow separation can be a highly important feature in river hydraulics (Leeder & Bridges, 1975). Flow separation changes the morphodynamics in a channel due to the changes in flow velocity it produces. In the area separated from the main flow the flow velocity is much lower and thus sedimentation is promoted. These changes in morphodynamics change the hydrodynamics, so a new local equilibrium between the hydrodynamics and morphodynamics is reached when flow separates in a sharp river bend. The effect is mostly the formation of a muddy counter-point bar and outer bank erosion.

Flow separation is a well-known and recognized phenomenon. It is however unknown in what conditions flow separates and which factors are important in the actual onset of separation (Kleinhans et al., 2010). Also Blanckaert et al. (2012) stated that there is a paucity of data and insight in the mechanisms of, and controls on flow separation and recirculation at natural sharply-curved river bends. This fact calls for further investigation of flow separation in sharply curved river bends.

To understand the phenomenon of flow separation it is necessary to recognize all relevant flow structures in sharp-bend-flow. Some basic mechanisms in sharp-bend-flow are the same as in straight-channel-flow. The main hydraulic characteristics that describe straight-channel-flow are: roughness, hydraulic radius, slope and the logarithmic velocity profile. In addition to these parameters and characteristics the other structures that are important in sharp-bend-flow are helical flow, flow separation and sediment-separation interaction. Helical flow is a structure that plays a part in every bend-flow, sharp and gentle bends, and flow separation occurs only in sharp-bend-flow. It appears that the chance of flow separation increases with increasing bend tightness and increasing Froude number (Leeder & Bridges, 1975), but it is unclear what all relevant internal processes and parameters of influence are. The effects of flow separation are: it creates vortices, flow contraction and it can cause flow recirculation. The “normal” flow-sediment interaction in straight channels is changed in sharp-bend-flow by helical flow and flow separation and thus the erosion and deposition are changed (Kleinhans et al., 2009).

1.1 Helical flow

Center region cell, spiraling flow, helicoidal flow or helical flow are names for the same phenomenon. It is the most pronounced secondary flow structure that is produced in sharp-bend-flow. According to Leeder & Bridges (1975) it is generally assumed that downstream flow through meander bends is helical and is accompanied by a transverse bottom flow component directed towards the inner bank. So every bend will cause helical flow to occur. This is confirmed by the observations in the experiment of Blanckaert and de Vriend (2004), where the center-region cell is the “classical” helical motion that is characteristic of flow in bends.

According to Blanckaert (2011), the center-region cell redistributes the velocity and causes it to increase toward the outer bank. This makes helical flow an important mechanism to understand sharp-bend-flow, flow separation and flow-sediment interaction in bends. Flow separation also redistributes the velocity in a bend, the connection between helical flow and flow separation is however not yet thoroughly understood. So further research needs to be done to understand flow separation, helical flow and the connection between the two.

Due to the inertia the flowing water has the tendency to flow straight, but the topography steers the flow to follow a depression in the landscape. Curving the water causes a centrifugal force that is directed to the outer bank in line with the center of rotation. The result of this is a transverse tilting of the water level and therefore a transverse pressure gradient with higher pressures near the outer bank than near the inner bank. The transverse pressure gradient thus accelerates the flow towards the inner bank. The transverse pressure gradient is competing with the centrifugal force in transverse movement of water in the stream. So the formation of helical flow can be explained by the local imbalance between the centrifugal force and the transverse pressure gradient (Blanckaert and de Vriend, 2004).

The roughness-induced logarithmic velocity profile induces the centrifugal force in the upper part of the water column to be larger than at the bottom. The centrifugal force wins from the transverse pressure gradient in the upper part of the water column and the transverse pressure gradient wins from the centrifugal force in the lower part. The result is that the water in a sharp bend enters a helical motion, this is a secondary flow structure. The greater the difference in streamwise flow velocity between the top and bottom section of a stream, the more pronounced the helical flow structure will be. Roughness is thus an important parameter, because it greatly influences helical flow due to the logarithmic velocity profile. And thus sharp-bend-flow structures can be expected to depend on the roughness parameter.

In figure 3 a conceptual sketch, by Blanckaert (2011), of the relevant processes in meander bends is given, showing:

- the logarithmic profile in depth of the streamwise velocity;
- helical flow: the transverse velocity directed towards the outer bank in the upper part of the water column and directed towards the inner bank in the lower part;
- the core of high streamwise velocity near the outer bank;

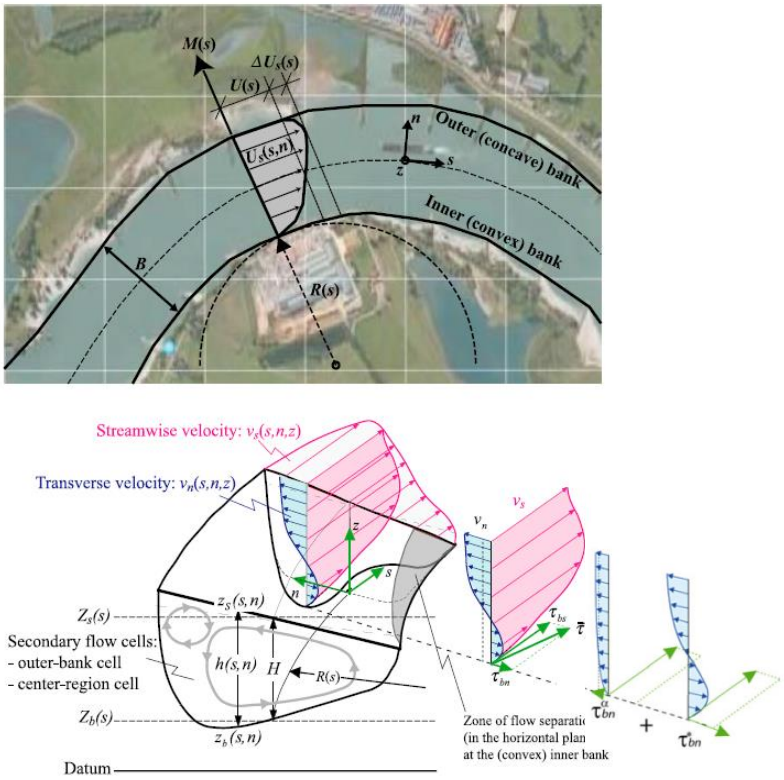

Figure 3, Conceptual sketch of the relevant processes in meander bends, definition sketch of the reference system, the most relevant variables and decomposition of transversal velocity. (Blanckaert & de Vriend, 2010 and Blanckaert, 2011)

1.2 Flow separation

According to Clancy (1975) and Anderson (2004) flow separation occurs, in aerodynamic situations, when the boundary layer travels far enough against an adverse pressure gradient that the speed of the boundary layer relative to the object falls almost to zero. This theory could provide insight in the hydraulic version of flow separation in sharp river bends.

Flow separation is mostly observed in sharply curved river bends. Straight channels do usually not show flow separation, except for when it is bedform- or construction-induced. In the case of a typical river bend three distinct boundary layers can be distinguished: the inner bank, the outer bank and the river bed. The location where flow can become separated and horizontal circulation cells can be formed is either just upstream of the bend apex at the concave (outer) bank, or just downstream of the apex at the convex (inner) bank (Hodskinson and Ferguson, 1998 & Kleinhans et al., 2009). In this literature study the bedform-induced flow separation is not discussed.

Although the same physical principals act in both boundary layers, the inner-bank flow separation differs from the outer-bank flow separation in the hydrodynamic causes and effects. In Figure 4 a photo is shown of an experimental setup that induces inner and outer bank flow separation to occur. In Figure 4 the zone of flow separation has been defined by the occurrence of an internal shear layer as identified by the occurrence of an inflexion points in the streamwise velocity patterns (Blanckaert, 2011). It can be seen that the extent and shape of the shear zones differs greatly, therefore also the hydrodynamic processes can be expected to differ greatly between inner and outer bank flow separation.

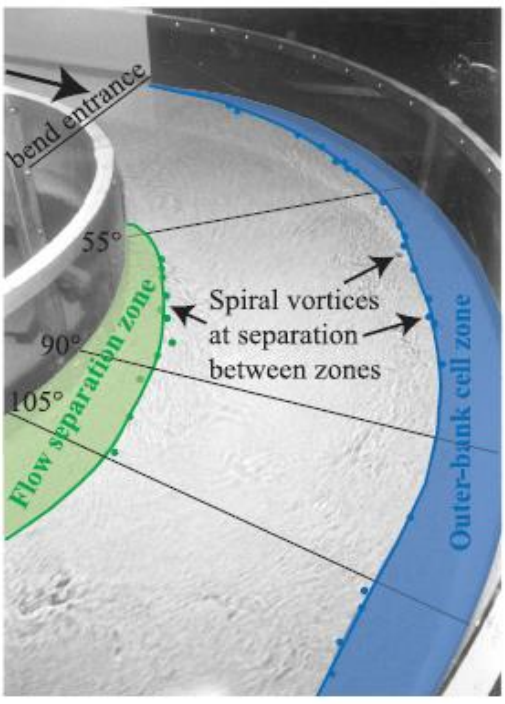

Figure 4, Visualization of the flow separation zone at the inner bank and the region covered by the outer-bank cell. (Blanckaert, 2011)

1.2.1 Hypothetical parameters of influence

The occurrence of flow separation possibly depends on the parameters discussed in the following section. These will be studied, tested and discussed in this review to gain insight in the mechanisms underlying flow separation.

The geometry of a channel defines the flow structures in a stream. Hence the geometry might also influence the chance of flow separation and the extent of flow separation. The geometry parameters are:

- Channel
    - Upstream channel planform
    - Streamwise variation in curvature
    - Flow depth
- Inner bend bank
    - Steepness of the bank
    - Curvature
    - Point bar form
- Outer bend bank
    - Steepness of the bank
    - Curvature
    - Widening / Flow expansion
    - Counter point bar form

The complex hydrodynamics in bend flow can cause flow separation to occur. The following hydraulic parameters may play a role in processes that cause flow separation to occur or influence the extent of flow separation:

- Froude number
- Roughness
- Turbulence
- Interaction of hydraulics with mobile bed
- Interaction of different flow structures

1.2.2 Hypothetical internal processes

The adaptation length may correlate with the location of the shear layer near the inner and outer bank, because straight channel flow needs a certain length to adapt to curved flow. The relation between the adaptation length in meters and several variables is given as:

$$\lambda_w = \frac{C^2 H}{2g} \quad (1)$$

where C = Chézy coëfficiënt ($\sqrt{m}\, s^{-1}$) and H = mean flow depth (m) (Struiksma et al., 1985) and (Kleinhans & Van den Berg, 2011). This equation shows that whether the flow in a bend is in equilibrium or not can be assumed to depend on roughness and actual water depth. So, an increase in water depth will move the bend flow structures downstream. A decrease in roughness has the same effect. So the location where flow separation starts in a bend may be predicted by the roughness and flow depth. Also the length necessary for the decay of the bend flow structures downstream of a bend may be predicted by this equation.

The streamwise water surface gradient $\left(\frac{\partial z_s}{\partial s}\right)$ is calculated by:

$$\frac{\partial z_s}{\partial s} = -C_f Fr^2 \left[1 + \alpha_{superelevation} \frac{H}{C_f B} \frac{\partial}{\partial s} \left(\frac{B}{R}\right) n\right] \quad (2)$$

where Cf = Dimensionless Chézy coefficient (-), Fr = Froude number (-), αsuperelevation = transverse tilting of the water surface (-), H = mean flow depth, B = channel width (m), R = centerline radius of curvature (m), n = transverse coordinate (m), zs = water level (m) (Blanckaert et al., 2012).

The streamwise water surface gradient in straight channel sections is given by: $(-C_f Fr^2)$, in square brackets the terms are stated that represent the effect of the curvature-induced transverse tilt. The streamwise water surface gradient is an important parameter in bend flow structures (Blanckaert et al., 2012). Therefore this equation provides insight in what parameters have influence on the formation of flow separation in bend flow.

Flow separation is caused by the abrupt changes in curvature. When the, curvature-induced, transverse tilt returns to a flat transverse water level an adverse pressure gradient may form near the inner bank. An adverse pressure gradient leads to flow deceleration and thus flow separation, when the flow deceleration is large enough the water will move upstream and may recirculate. The parameters in square brackets influence the formation of flow separation, because they represent the curvature-induced transverse tilt and thus the possible formation of adverse pressure gradients.

Concluding, the main parameters of influence on flow separation are H/B, Cf and streamwise change in B/R. An increase in H/B (deeper), a decrease in Cf (rougher) and a streamwise increase in B/R (sharper) will result in more chance of flow separation. Inner bank flow separation is most likely to be influenced by these parameters, but flow separation near the outer bank is also likely to be influenced by the transverse tilting of the water surface.

1.2.3 Hypothetical causes

Inner-bank flow separation has been investigated to a surprisingly low degree. The available fundamental knowledge about the associated hydrodynamics is vague and sparse, often not describing fundamental physical processes. For example, Bagnold (1960) stated that a stage must be reached at which the flow in a river along the inner boundary becomes unstable and breaks away from the boundary, leaving an intervening space occupied by a zone of unstable and confused motion. In figure 5 a sketch shows inner-bank flow separation starting in a meander bend causing recirculating flow, a decrease in effective flow width (flow contraction), vortices and the downstream decay of recirculation and vorticity. Blanckaert (2011) has shown in an experiment that this weakening of the separation zone is accompanied by its widening, so the velocity difference between the flow separation zone and the main flow body and the corresponding inflexion point in the transverse velocity profiles become less pronounced and have almost vanished at the bend exit.

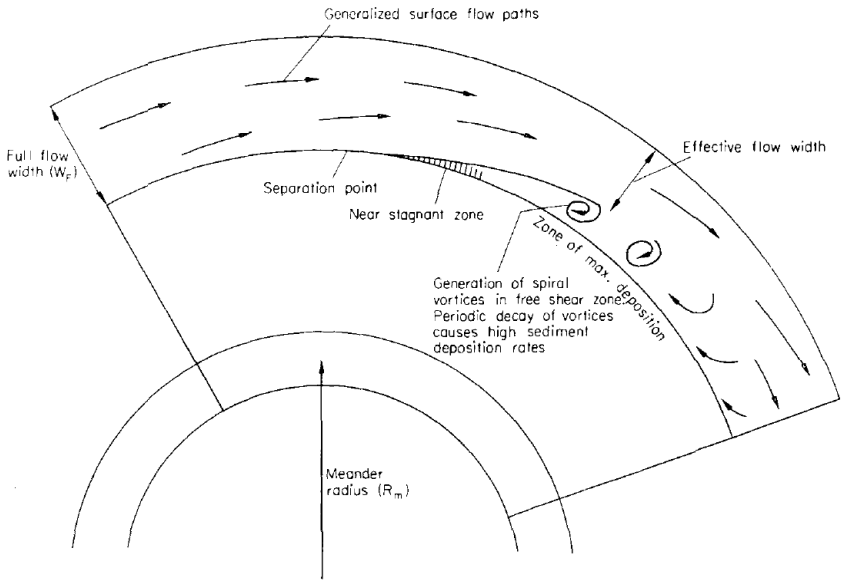

Figure 5, Sketch of the main characteristics of flow separation in a meander bend. (Bridges & Leeder, 1976)

The flow does not separate directly at the beginning of the bend, as can be seen in the sketch in figure 5. The experiments of Blanckaert (2011) showed that the flow separates from the inner bank at about 40° in the bend. This is a typical location where flow separation starts and it may be influenced by the adaptation length (1), but there is no conclusive answer as what determines the location where flow separation starts.

Studies have been done to examine the relation between flow separation and several parameters of influence. According to Leeder and Bridges (1975), flow separation is best expressed as a function of bend tightness and Froude number, whereby an increase in bend tightness and Froude number promote flow separation. Bend tightness is defined as the dimensionless ratio between meander radius (R) and flow width (B). Bend tightness and Froude number are representative parameters for all channel sizes, because they have approximately linear relationships to channel size.

Note that Froude number and bend tightness are also used in equation (2). So the relation between bend tightness, Froude number and flow separation, described by Leeder and Bridges (1975), agrees with the later described relation of Blanckaert (2011), because the sudden vanishing of the transverse tilting of the water level is curvature-induced, so both articles state that bend tightness is an important parameter in relation to flow separation. Hickin (1977) suggested a curvature of R/B <= 2 is required for inner bank flow separation to occur.

The onset of flow separation also appears to be a steeply decreasing function of Froude number as meander bends become less tight (Leeder & Bridges, 1975). This means that a tight bend only needs a low Froude number and a gentle bend needs a high Froude number for flow separation to occur. Leeder & Bridges (1975) state that their results indicate that flow separation is possible in a range of meanders at quite modest Froude numbers (0.27-0.42). However, Bagnold (1960) rejected the use of the Froude number, because separation in pipes is similar to separation in open-channel flows, but Fr can only be defined for open-channel flow. So the relation of the Froude number to flow separation should be investigated further.

Channel roughness plays an important role in sharp bend flow. Channel roughness causes the boundary layer to be thicker and slower, this makes the fluid near the bank more susceptible to adverse pressure gradients and therefore the chance of flow separation is likely to increase with increasing channel roughness. In addition, the roughness (or a perturbation-induced flow instability) leads to turbulence. And turbulence plays an important role in the generation of inner-bank flow separation (van Balen et al., 2010). The position of the separation point however is independent of the Reynolds number (Schlichting & Gersten, 2000).

Little is known about turbulence in sharp bend flow, because it is hard to measure and model. Turbulence is even noted in the Open Questions in Physics by Baes (2012) as a phenomenon that is not understood and the effects cannot be calculated. It is however clear that flow separation and the associated shear layer create turbulence, mostly in the form of vortices and eddies. Turbulence may help in generating flow separation and flow separation creates turbulence, so the interrelation is complex.

Flow separation near the outer bank is very different from inner-bank flow separation. The causes and internal processes of flow separation near the outer bank are better understood than near the inner bank. In Figure 6 a sharp bend that induces a classic case of outer bank flow separation is shown, the outer bank flow recirculation is extensive. Also inner bank flow separation and recirculation occurs in this bend. Note that flow velocity is measured at the surface and at 0.3 m depth, both measurements show separation and recirculation near the outer and near the inner bank.

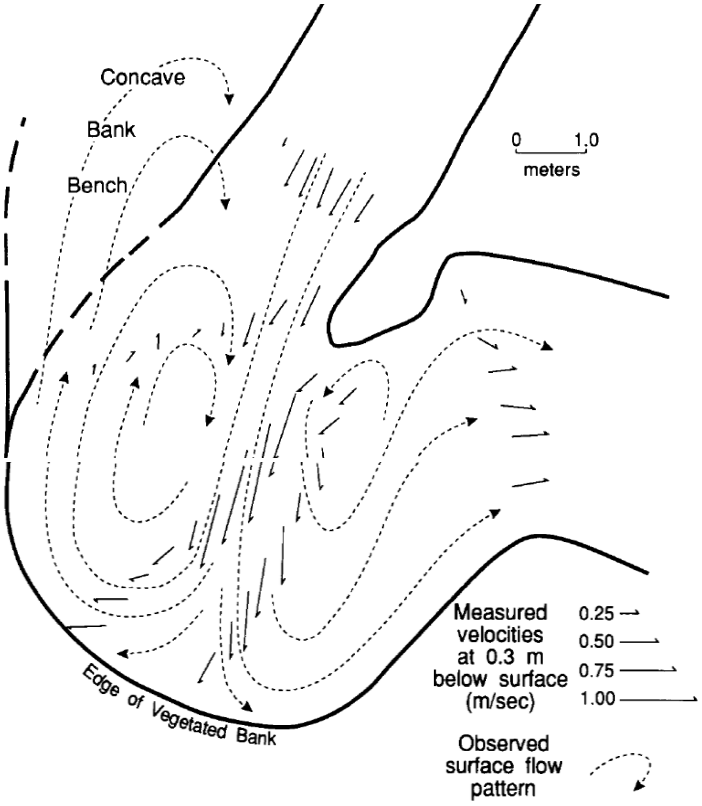

Figure 6, Measured flow velocities and directions at 0.3 m depth and observed surface flow pattern. (Andrle, 1994)

For the outer bank also studies have been done to examine the relation between flow separation and several parameters of influence. The planform or morphology of a stream is an important factor for the hydrodynamics, this makes planform a significant factor determining the phenomenon of outer bank flow separation. Firstly, outer-bank flow separation amplifies with *increasing steepness of the outer bank* (Blanckaert, 2011). Secondly, it amplifies especially with *increasing bend tightness* (Blanckaert, 2011) & (Hodskinson and Ferguson, 1998). Thirdly, Hickin (1977), Page and Nanson (1982) and Hodskinson & Ferguson (1998) proposed that *channel widening* at the apex of a sharply curving bend facilitates flow expansion and allows separation to develop at the outer bank (Figure 6 also shows this fact). So the term planform can be distinguished in three main parameters that determine outer bank flow separation. But more facts have also been found to influence outer bank flow separation, such as the form of the point bar within the bend and the planform of the upstream channel (Hodskinson and Ferguson, 1998). However these variables are hard to parameterize.

Turbulence is an important factor in the generation of outer bank flow separation (Blanckaert and de Vriend, 2004). Turbulence can promote outer bank flow separation by kinetic energy input. Yet, there is little insight available into the dynamics of the turbulence in the vicinity of the outer bank flow separation, and even the causes are almost unknown (Blanckaert and de Vriend, 2004). The flow instability and turbulence can be planform-induced, so planform is a factor that influences outer bank flow separation via two processes. This makes planform a very important factor in understanding outer bank flow separation.

In addition to planform, roughness is an influence on turbulence and flow instability which in term influences outer bank flow separation. According to Blanckaert (2011) outer bank flow separation strengthens and widens considerably with increasing roughness of the outer bank.

1.2.4 Effects of flow separation

Flow separation comes with several phenomena:

- Flow recirculation in the separated zone
- Contraction of the main flow
- A shear layer (the definition of flow separation)
- Vorticity-induced by the shear layer
- Interaction of the different flow structures mentioned above
- Separation-sediment interaction

Below I discuss these effects in detail.

The water in the separated zone, near the outer or inner bank, receives little kinetic energy input from the main flow. This causes the separated zone to be more susceptible to kinetic energy input from processes which may move the water in the opposite direction of the main flow. This flow reversal can lead to flow recirculation.

The zone of flow reversal in Figure 5 and Figure 7 can be called an open separated zone, because the shear layer does not fully surround a part of the flow. In the case of a closed separated zone, as can be seen in the outer bank separation zone in Figure 6, the shear layer starts and ends at the inner bank with little water transfer between the separated zone and the main flow. In this case the separated water is driven by the shear layer and thus recirculates. Flow recirculation can only happen when the separated zone is closed, in an open separated zone flow reversal can occur, but not recirculation.

An absolute water surface increase in the downstream direction leads to an increase in static pressure in the same direction. This adverse pressure gradient may be a factor which causes flow recirculation, because the adverse pressure gradient causes a deceleration of the streamwise flow. This deceleration is mostly relatively small compared to the main flow velocity, not being able to reverse the flow. In the separated zone however, when the steamwise velocity component is small enough, the adverse pressure gradient can be large enough to cause flow reversal. Which may result in flow recirculation.

Near the inner bank the cause of recirculation typically is an adverse pressure gradient caused by the sudden vanishing of the curvature-induced transverse tilting of the water surface (Blanckaert 2011). Near the outer bank a sudden increase in the transverse tilting of the water surface causes an adverse pressure gradient. The flow in the sluggish separated zone can therefore be decelerated. The kinetic energy input in the outer bank separated zone is relatively large compared to the inner bank separated zone due to the inertia-induced impinging of the main flow on the outer bank. The adverse pressure gradient is therefore less likely to be large enough to reverse the flow.

In bends with outer bend widening flow recirculation is not only caused by a curvature-induced transverse tilting. The widening-induced flow expansion causes reduced downstream slope and flow deceleration (Bridge, 1993). This flow deceleration may induce flow recirculation.

Because the part of the stream with sluggish water does not take part in the downstream transport of water the main flow is contracted and flow velocity in the main stream is increased. Leeder & Bridges (1975) observed effects of flow separation in their study reaches. One of them was a decrease in effective flow width downstream of the separation point of up to 50% (visualized in Figure 4 and Figure 7). Thus increasing the flow velocity in the main part of the stream and increasing the erosive effect,

forming a scour pool. Ferguson et al. (2003) found that the reduced effective flow width is more than offset by an increase in flow depth. So effectively the flow is contracted horizontally due to flow separation and expands in a vertical direction. During this process the effective width is reduced considerably and the flow is concentrated in the outer half of the cross section (Blanckaert, 2011).

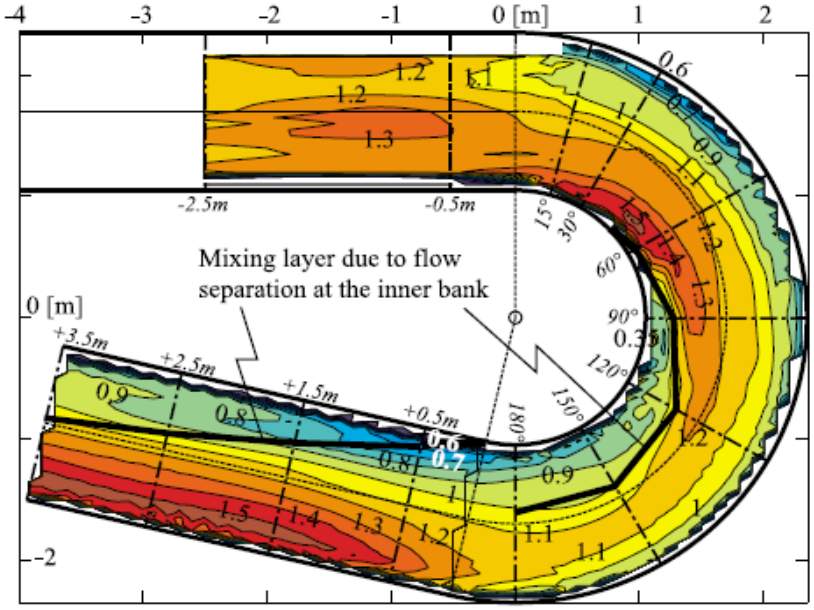

Figure 7, Distribution of the normalized streamwise velocity at the water surface around the flume. The edge of the flow separation zone was determined from the inflexion point in the transverse distribution of the streamwise velocity at the water surface. (Blanckaert, 2011)

When a shear layer reattaches downstream with the bank it separated from, it fully separates a zone from the main flow, this can be called a "closed" zone. In case of a mobile, natural river bed the flow separation-sediment interaction caused a "closed" zone of flow recirculation to occur in the experimental setup of Blanckaert (2011). In the case of a horizontal river bed (Figure 7) the flow separation showed a streamwise widening, it had a transverse extent of about four times the water depth at the bend exit, thus contracting the flow considerably (Blanckaert, 2011).

Flow separation causes a sharp transition in flow velocity, this sharp transition acts as a shear layer that periodically causes complex three-dimensional vortices and eddies to occur. The complex eddy systems are spinning fluid particles that can be described by the term vorticity. Vorticity is a feature that partly describes turbulence and it is a measure of moment of momentum of a small spherical fluid particle around its own center mass. This fact show that flow separation can be located by identifying regions with high vorticity.

The vorticity decays as the separation zone merges back into the general downstream flow at the meander inflection point (Leeder & Bridges, 1975). This downstream decay of the shear layer and the decay of the spiral vortices is caused by viscosity. The viscosity causes kinetic energy transfer from the main flow to the separated zone, thus diffusing the transverse gradient in streamwise flow velocity. The diffusing of the transverse gradient causes the flow to gradually return to a classical straight channel flow with a logarithmic velocity profile and the core of high flow velocity in the middle of the flume.

In addition to the shear layer, the centrifugal force can also generate vorticity, which is local rotational energy. And in the case of the near-bank cells in straight uniform flow, turbulent shear stresses are also responsible for the generation of vorticity (Blanckaert and de Vriend, 2004). Vorticity can be dissipated by the turbulent shear stress and/or the molecular viscosity (Blanckaert and de Vriend, 2004). So it is not clear a priori whether locally the turbulent shear stresses in total increase or decrease the mean vorticity (Blanckaert and de Vriend, 2004).

The above mentioned flow structures can influence each other. For example the remnants of a helical flow structure from an upstream bend can influence the formation of flow separation in the downstream bend. Blanckaert et al. (2012) state that the generation of flow separation near the second outer bend is favoured by the remnants of the helical flow of the upstream bend. Inner bank flow separation is however counteracted by helical flow remnants.

In a river, the hydrodynamics and the morphology are interdependent upon each other. Flow separation redistributes the flow in a bend, the velocity in the main flow is increased and the separated zone is moving sluggishly. Causing sedimentation in the separated zone and erosion in the main flow. In braided rivers this means: enhanced deposition on the downstream tips of braid bars and side bar adjacent to confluence scour zones, thereby reducing the effective local cross-sectional area of the channel (Bridge, 1993). This change in planform influences the hydrodynamics and thus flow separation. Resulting in a complex interaction of flow separation and morphology. Bridge (1993) however states that flow separation enhances deposition on side bars rather than being the sole cause for their occurrence. So in the interaction flow separation is likely to be more dominant than the changes in morphology it causes.

The main effect of inner bank flow separation-sediment interaction is the formation of a muddy, smooth, low sloping and soft point bar and a scour pool in the outer bend (Kleinhans et al., 2009). It should be noted that these observations were done on an intertidal flat, but the general effects can be assumed to happen in all sharp river bends.

The flow separation-sediment interaction causes a “closed” instead of a streamwise widening zone of flow recirculation in the case of a horizontal bed. The low-velocity recirculating flow in the shear zone is efficient in trapping sediment that builds up the point bar and promotes inner-bank accretion (Blanckaert, 2011), thus creating a muddy, smooth, low sloping and soft point bar. A muddy point bar may accrete up to 20 mm of suspended sediment in one ebb/flood cycle (Leeder & Bridges, 1975). So flow separation is a significant process that greatly influences the morphology in intertidal areas.

The flow separation leads to flow contraction, which in terms leads to an increase in flow velocity and thus an increase in erosion, resulting in a scour pool near the outer bank and enhanced velocities near the toe of the outer bank (Blanckaert, 2011). Bagnold (1960) argued that this happens because the relative roughness of the channel is less than over the shallow inner bank zone. The enhanced velocities near the toe of the outer bank promotes erosion of the outer bank, so inner bank flow separation induces outer bank erosion. The results of the study of Blanckaert (2011) also suggested that inner-bank flow separation enhances meander migration. But its dependence on curvature and shallowness remains unknown (Blanckaert, 2011). Kleinhans et al. (2009) observed the flow through the thalweg separated from the inner bend and impinged on the outer-bend bank downstream of the apex, where bank erosion was focused.

At the outer bank the process is different. Helical flow redistributes the velocity and causes it to increase toward the outer bank and the outer bank flow recirculation prevents this increase to continue through to the bank and keeps the core of maximum velocity a distance from the bank at the separation layer (Blanckaert, 2011). Outer bank flow recirculation therefore protects the outer bank from the increased flow velocity and erosion due to helical flow and inner bank flow separation.

Outer bank flow recirculation strengthens and widens considerably with increasing roughness of the outer bank, indicating that their protective effect may be more important in natural meander bends with irregular rough banks than in laboratory or numerical experiments (Blanckaert, 2011). However outer bank flow recirculation and outer bank roughness may be influenced by flow separation-induced counter point bar formation. Roughness thus influences flow separation by influencing the complex balance between morphology and hydraulics.

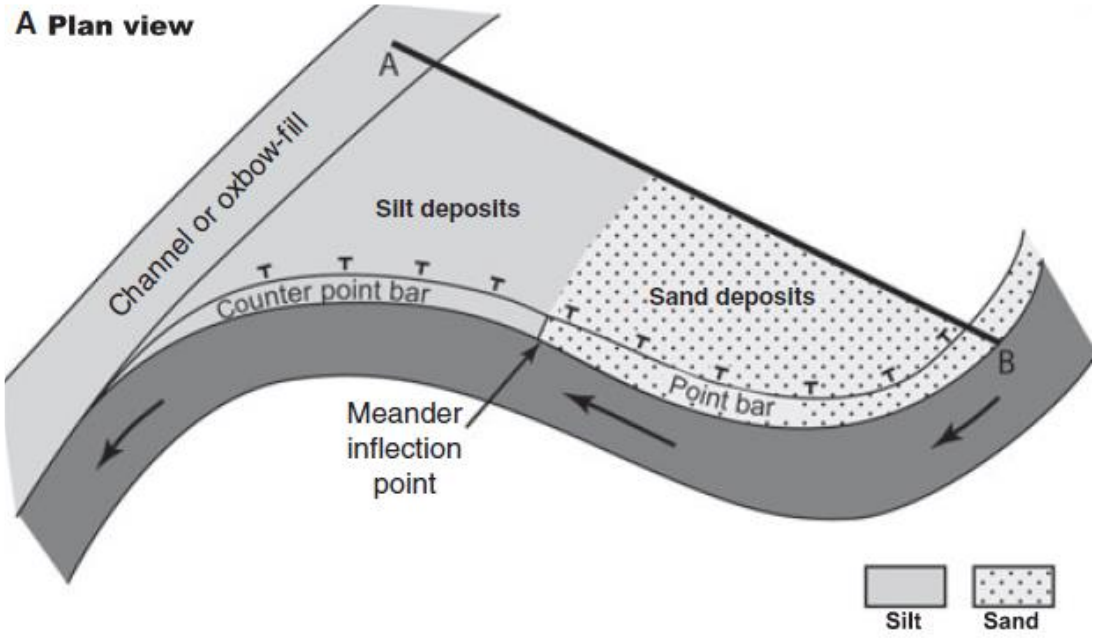

Figure 8, Proposed silt-dominant counter-point bar lithofacies model for large, mixed load, low gradient, sand bed, meandering rivers, summarized from the results of the study of Smith et al. (2009) (Smith et al., 2009)

In addition to the protective effect of the outer bank flow separation, it also induces a counter point bar to form. Figure 8 shows the location of the point bar and the counter point bar, the counter point bar is concave in plan form and is a transition and continuation from point bars that extend to the valley side (Smith and Pearce, 2002). It is formed by the decreased flow velocity and reverse eddy currents moving upstream in the outer bank flow separation zone. Mostly fine grained and organic sedimentation occurs at high flows in the separation zone (Nanson and Croke, 1992). According to Smith et al. (2009) reverse eddy currents and scour pools can be formed due to flow separation when a river is forced to make an abrupt 90° or sharper bend (120°). Smith et al. (2009) however do not state which degree of curvature, mostly defined as a ratio between stream width and bend radius, can be defined as an abrupt bend. So it is clear that reverse eddy currents and scour pools form in sharp bends due to flow separation, but the exact causes and processes are not known.

1.3 Review

In sharp-bend-flow there are two additional hydrodynamic phenomena that are different from normal channel flow, these are: helical flow and flow separation. Helical flow causes the flow velocity to be directed towards the outer bank in the upper part of the water column and directed towards the inner bank in the lower part. Flow separates, near the inner bank, due to the sudden vanishing of the curvature-induced transverse tilting of the water surface. Flow depth and roughness also have an influence on the transverse tilt and thus on flow separation. Near the outer bank the flow is likely to separate due to bank roughness, outer bend widening and possibly the transverse water surface tilting at the bend entrance.

The effects of outer- and inner-bend flow separation are flow recirculation, contraction of the main flow, a shear layer, shear layer-induced vorticity, interaction of before mentioned hydraulic phenomena and separation-sediment interaction. These flow separation-induced hydraulic phenomena have major morphological effects. It creates a scour pool near the outer bend that may cause outer bank erosion. Outer bank flow separation can however protect the outer bank from erosion and create a counter point bar. Also inner bank flow separation causes a point bar to form and the core of high flow velocity to move toward the outer bank, promoting outer bank erosion.

The exact causes and internal processes of inner bank flow separation remain unknown. According to the papers discussed in this report several parameters cause or influence flow separation. All quantifiable parameters, mentioned below, have a positive feedback on flow separation.

Firstly, the following initial conditions, these are all geometrical parameters, are proposed to be a cause of flow separation:

- ***Channel***
  - **Upstream channel planform** (Hodskinson and Ferguson, 1998)
  - **Streamwise increase in curvature $\frac{\partial}{\partial s}$(B/R),** influencing transverse water surface tilting (Leeder and Bridges, 1975), (Hodskinson and Ferguson, 1998), (Blanckaert, 2011), (Blanckaert et al., 2012)
  - **Flow depth (H),** increasing adaptation length (Struiksma et al., 1985) and (Kleinhans & Van den Berg, 2011)
- ***Inner bend bank***
  - Curvature needed to induce inner bank flow separation: R/B <= 2 (Hickin, 1977)
  - **Flow depth (H/B),** influencing transverse water surface tilting (Blanckaert et al., 2012)
  - **Point bar form** (Hodskinson and Ferguson, 1998)
- ***Outer bend bank***
  - **Inclination of the bank (°)** (Blanckaert, 2011)
  - **Flow expansion at the apex** (Hickin, 1977), (Page and Nanson, 1982) and (Hodskinson & Ferguson, 1998)

Secondly, the following internal processes, these are mostly hydraulical parameters, are proposed to have an influence on flow separation:

- **Froude number** (Leeder & Bridges, 1975)
    - However, (Bagnold, 1960) rejected the relation between Froude number and flow separation
- **Roughness**
    - **Outer bank roughness** (Blanckaert, 2011) (More important in natural than in numerical or experimental settings)
    - **Channel roughness,** increasing adaptation length (Struiksma et al., 1985) and (Kleinhans & Van den Berg, 2011)
      influencing transverse water surface tilting (Blanckaert et al., 2012)
      influencing boundary layer flow velocity and thickness
- **Turbulence,** promotes inner- (van Balen et al., 2010) and outer- (Blanckaert and de Vriend, 2004) bank flow separation.
    - Note, there is a complex interrelation between flow separation and turbulence.
- **Interaction of different flow structures**
    - **Outer bend flow separation and inner bend flow separation**
    - **Remnant helical flow structure of upstream bend,** opposes the onset of inner-bank flow separation and favors the generation of an outer-bank cell or flow separation (Blanckaert, et al., 2012)

According to several papers the following effects are commonly associated with flow separation:

- Flow recirculation in the separated zone
- Contraction of the main flow
- A shear layer
- Vorticity induced by the shear layer
- Interaction of the different hydraulical effects mentioned above
    - Planform or roughness may cause turbulence, which in terms can influence flow separation
- Separation-sediment interaction
    - Inner bank flow separation induces the formation of:
        - A scour pool (Ferguson et al., 2003) (Kleinhans et al., 2009)
        - A point bar (Ferguson et al., 2003) (Kleinhans et al., 2009)
        - Outer bank erosion (Blanckaert, 2011)
    - Outer bank flow separation:
        - Induces the formation of a counter point bar (Smith and Pearce, 2002)
        - And protects the outer bank for erosion (Blanckaert, 2011)

1.4 Problem definition and research goal

Firstly, studying flow separation is necessary in order to understand the controls on the development and persistence of flow separation. Secondly, flow separation research is needed to understand the associated deposition and erosion in individual bends, to predict meander migration (Blanckaert, 2011). Thirdly, flow separation research is needed to the predict effects of channel change on the onset and extent of flow separation (Hodskinson and Ferguson, 1998).

So, according to me, the remaining knowledge gaps that need to be studied are:

- What curvature is needed to induce flow separation?
- Is Froude number a parameter of influence? If so, what is its relation to flow separation?
- What is the relation of roughness to flow separation? What is the interrelationship between:
    - Transverse tilt
    - Adaptation length
    - Turbulence
- What is the relation between flow separation and helical flow? (upstream remnants?)
- What is the relation of planform to flow separation?
  The aspects of planform are:
    - bend length
    - flow depth (also in relation to width and scour pool)
    - distance between bends
    - point bar shape
    - inclination of inner bank
    - inclination of outer bank
    - outer bank widening

2 Methods

Existing experimental laboratory data-sets were analyzed, the data-sets were created in the Hydralab III experiment by Kleinhans et al. (2010) and Blanckaert et al. (2012). These data-sets have not yet been fully analyzed or published. The data-sets that were used in this report comprise mainly LS-PIV (Large Scale Surface Particle Image Velocimetry) measurements. "FlowScout" image analysis software was used to create raw, time averaged surface vector flow fields. The FlowScout output data was analyzed using Matlab. In Matlab many ways of plotting and presenting the data were used.

2.1 Experimental data-sets (Blanckaert et al., 2012):

For the Hydralab III experiment a Plexiglas flume was constructed in the Total Environment Simulator (TES) at Hull University. In Figure 9 the map of this flume is given. The curved flume had a width of 1 meter and two bends with radii of 1 and 2 meter for the first and second bend respectively. The discharge and basin water level were controlled and measured. Pressure sensors recorded water level along the flume. The flow structures in both bends were measured with surface PIV, an ADV array, 3DPIV and ADVP (Kleinhans et al., 2010). Measurement techniques that could influence each other were not performed simultaneously. The legend in the insert in Figure 9 provides information on the location of the measurements by means of pressure transducers, Large Scale Surface Particle Image Velocimetry (LS-PIV), three-dimensional Particle Image Velocimetry (3D-PIV), an Acoustic Doppler Velocity Profiler (ADVP) and a manual point gauge (bed and water surface levels). Most Hydralab data-sets are open and can be requested for analysis.

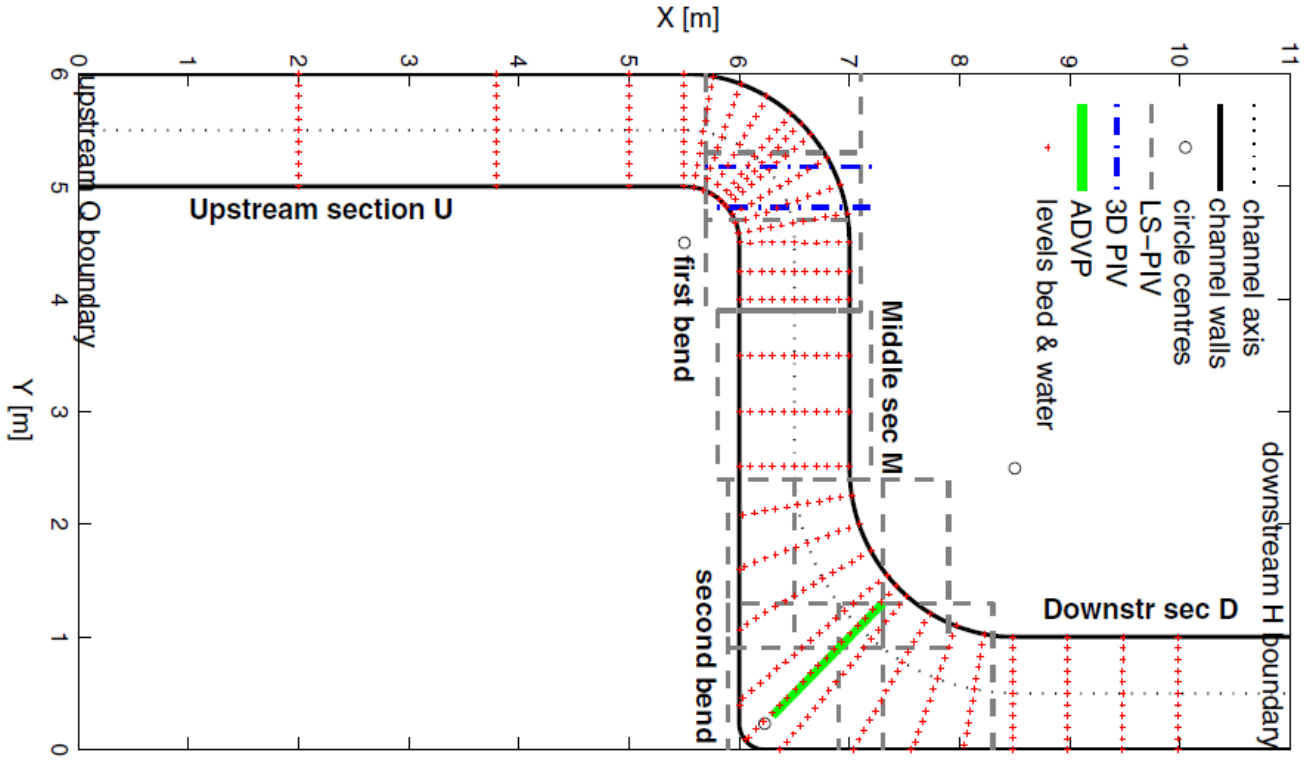

Figure 9, Map of the bespoke flume channel. Flow is from bottom to top (scale in meters). Circular bends were constructed from Perspex (Blanckaert et al., 2012).

Three scaling conditions were posed for the fixed bed. First, the Shields number was below critical for motion. Second, the Froude number was smaller than unity (subcritical flow). Third, the backwater adaptation length was of the order of the flume length so that the gradient is controllable by the downstream water level, and the flow should be uniform. For experiments with much lower Froude number the condition of uniform flow was relaxed. The experiments on fixed bed show that Chezy number is constant rather than Nikuradse roughness length despite the immobile bed (Kleinhans et al., 2010). In the experiment the flow depth and the Froude number were changed to create 6 different general flow conditions, which is given in Table 1. This made it possible to analyze the influence of flow depth and Froude number on flow separation. In this table also the Reynolds number and the hydrodynamic adaptation length is given.

Table 1, General flow conditions. Width of the flume is 1.00 m. Gradient of gravel bed is $1x10^{-3}$ mm^{-1} and of sand bed is about $2\text{-}4x\ 10^{-3}$ mm^{-1} (Kleinhans et al. 2010)

experiments		Depth (m)	Froude nr. (-)	Chezy ($m^{½}s^{-1}$)	Reynolds nr. (-)	Adaptation length water (m)	Remarks
Small depth	**high Fr**	0.08	0.53	38	$3.7 * 10^4$	6.0	
Intermediate depth	**high Fr**	0.14	0.49	34	$8.1 * 10^4$	8.1	
Large depth	**high Fr**	0.20	0.50	34	$1.4 * 10^5$	12.0	
Small depth	**low Fr**	0.08	0.20	35	$1.4 * 10^4$	5.1	Non-uniform
Intermediate depth	**low Fr**	0.14					Non-uniform
Large depth	**low Fr**	0.20	0.16	36	$4.6 * 10^4$	13.4	Non-uniform

Every flow condition was given at least one number to identify the experimental conditions of the measured data. In Table 2 all flow condition numbers are given.

Table 2, Overview of experimental flow conditions

Flow conditions	Low Fr	High Fr
8 cm flow depth	1508*	0408 - 0708
14 cm flow depth	1414*	1314* - 1614(additional measurements) (Mobile bed: 1814 – 1914 – 2014 – 2114)
20 cm flow depth	0520 - 0820 - 1120#	0320 - 0620 - 0920 - 1920 – 1220#

* = LSPIV only, # = PIV only (not relevant in this report)

The surface flow structures in both bends were measured with LS-PIV at the water surface. Large Scale Surface Particle Image Velocimetry (LS-PIV) is a method to obtain detailed measurements to identify the gross, time averaged, flow structures in surface flow. White particles of 2 mm diameter and a density of 900 kgm^{-3} were seeded upstream of the measurement location and occasionally in recirculating zones. Lighting was introduced from downstream to upstream to minimize water surface reflection. The immobile gravel bed was spray-painted black within measurement locations to optimize image contrast. Images were collected perpendicular from above with a 1008x1018 8BPP CCD camera with an exposure time of about 4 to 20 milliseconds at standard or doubled gain (see appendix 9.1 for the exposure time and gain values used in the experiment), with the aim of deriving as sharp an image as possible. The field of view was approximately 1.3m by 1.3m and images were captured for two to three minutes at a rate of 15Hz.

2.2 LS-PIV analysis using FlowScout

FlowScout created flow vectors in the following steps. First a standard spectral correlation method to calculate flow velocity and direction was done in a grid. Particle tracking was then used to obtain velocity vectors for each particle, where the average velocity in the interrogation area was used to filter and prevent aliasing whilst allowing variation due to turbulence. This was enhanced with filter criteria for particle detection on an unevenly lighted background.

To optimize the functioning of FlowScout, many variables and settings in the software can be changed. Most of the following settings was experimented with in combination with the LSPIV dataset. In **bold black text** the name of the setting is given, in **bold red text** the used setting value is given followed by a short description.

- **Mask**, **always used.** The Mask was made in FlowScout and it was used to prevent vectors that were not located in the water to be identified.
- With/without **background**. **Mean background was always subtracted.** The background was made in FlowScout by calculating the mean of every pixel in all images with particles of one camera position in one flow condition. The analysis was then able to be executed with subtracting the mean image of every image before particle selection and particle tracking. This method resulted in less erroneous particles to be identified.
- With/without **pixel value threshold** (% or values from 0 to 256). **A lower threshold of 35 and an upper threshold of 256 was always used.** This setting prevented the identification of particles outside the pixel value threshold. So when set to: 35<pass<256, it results in the exclusion of particles that have a peak lower than 35. This was necessary, because most particles selected with a value below 35 were not really particles, but small waves that caused flickering. But particles may have be deleted by setting the lower threshold value too high, so there was an optimal value for the lower threshold, this might change between images, camera position, lighting conditions, flow conditions, etc.
- **Particle selection.** **Set to standard**
    - **Particle Identification.** **Set to 1.5 and 2.** This setting was based on intensity ratios and it was able to exclude clumps of particles. This was necessary because the clumps caused particle tracking to give erroneous vectors. Increasing the values, so moving the cross to the right and/or upwards, would have decreased the amount of particles identified and therefore decreased the amount of vectors in the output data. The particles that were not identified by increasing the values were particles that were very close to each other.
        - **Sensitivity.** **Medium** (high did not give good results)
    - **Phase Selection**, **not used** (experiments were done with this setting, but Dr. McLelland advised not to use it, because clumps of particles were not selected anyway) (personal communication, April 2013).
- **Time between images.** **This was always 0.0667 seconds (15Hz),** as the camera was always set to 15Hz.
- **Search distance.** (x [pixels], y [pixels]). Varies between camera positions **(see Appendi 9.1 for the values).** These values define the maximum distance FlowScout searches for particles between image pairs, so it defines the maximum magnitude of the output vector data. So they were as small as possible to exclude erroneous vectors that were faster than the flow in reality, and large enough to pick up the fastest real vector. The values were handpicked by looking at the pictures in sequence.

- **Tracking method. PTV (Particle Tracking Velocimetry).** PTV was advised by Dr. McLelland (personal communication, April 2013). The PTV method resulted in one vector per particle pair. Another option was the PIV-FFT method (Particle Image Velocimetry - Fast Fourier Transform).
- **Vector validation.** [pixels/s]. Varies between camera positions **(see Appendi 9.1 for the values).** The order of the values in the appendix are [minU, minV, maxU, maxV]. This setting excluded vectors that were faster or slower than actually possible. U-component was vertical in images, positive was up. V-component was horizontal, positive was to the right. After loading the data into Matlab this orientation will change.
    - **Dominant direction. not used.**
    - **Minimum magnitude.** A value of **0.2 pixels/s** (0.28 mms^{-1}) was always used to exclude nearly stationary vectors.

2.3 Vector field analysis using Matlab

The FlowScout output data was loaded into Matlab. The FlowScout output data of every camera position was called "BatchParticleInformation.dat". After loading the data, the data was transformed to a file structure that was easier to handle. Several columns of data, calculated by FlowScout, were not needed and were not loaded into Matlab, only the measured data was kept. The measured data comprises the location [x,y], magnitude [m] and direction [u,v] of the vectors and their timestamp [t]. After loading and transforming the new filename was "ParticleInformation.dat". The "ParticleInformation.dat" file was loaded into another Matlab script (called PIload.m) to do further analysis. The first step in this script was the repositioning of vectors to their correct location in the x-y coordinate system and the exclusion of spurious vectors.

All vectors of every camera position were converted to metric values, rotated, scaled and moved to the right place in the x-y coordinate system. FlowScout defines 1 pixel as 1 millimeter, the field of view of the camera was approximately 1.4 meter and the resolution was 1008x1018. The data (x,y,u,v,m) was multiplied by approximately 1.4 (there was variation between camera positions) to convert to metric values. This resulted in the (x,y) data to be converted to [meter] and the (u,v and m) data to be converted to [ms^{-1}]. The parameter (t) was defined as number of image pair, so t=0 was the analysis of image 0 and image 1. The unit of t is 1/15 second. By analyzing a raw image of every camera position the needed rotation of the data was determined and then applied to the data in Matlab. The correct position in the x-y coordinate system was determined by loading the data and matching the vectors to the flume boundaries, this was a trial and error process. The last step of the load procedure was the sorting of the vectors, so that x was in increasing order.

Variables.mat was loaded into Matlab, it contained three structure variables: *bound, g* and *xsec*. *Bound* contained the outlines of the flume and was used to delete all vectors that lay outside the flume. *g* contained the position of all gridline intersections of the grid (292*41) that was used to grid the vectors onto using median filtering. This curvilinear grid was made in Delft3D to make comparison with the Delft3D results easier. *Xsec* was not used in this research.

In PIload.m a script was used to delete spurious vectors. Spurious vectors were vectors that were likely to be caused or affected by hands, heads or airborne particles in the images. The script removes all the vectors that were created in every frame with a hand, head or airborne particle in it. The frame numbers were determined by hand, so by looking at every frame.

To improve the vector data, a script was used to exclude erroneous vectors. Grid cells with little vectors were mostly located in areas where reflections were observed, this fact implied that the little vectors in these grid cells were of low quality. Therefor a minimum amount of vectors per grid cell was given as a threshold. Grid cells with low quality vectors were also expected to have a larger standard error in magnitude than good quality grid cells. So, a maximum standard error of magnitude was given as a threshold. The standard error was calculated by dividing the standard deviation of the magnitude of all vectors in a grid cell by the square root of number of vectors in that grid cell:

$$SE_{gc} = \frac{\sqrt{\frac{\sum(M_{gc}-\overline{M}_{gc})^2}{n-1}}}{\sqrt{n_{gc}}} \quad (3)$$

So grid cells with less than the minimum amount of vectors or with a higher standard error of magnitude than the given thresholds were replaced with NaN values. This filter step resulted in gaps in the plots where data quality was low. For the sake of comparing the results of different flow conditions constant thresholds were used for all conditions. The thresholds were: Nthres = 100 and SEthres = 0.03, where Nthres was the threshold that defined the minimum amount of vectors and SEthres was the maximum allowed standard error of magnitude.

2.4 Shear layer detection

The vector field analysis resulted in maps of measured surface flow structure, maps of calculated vorticity and deduced simplified shear layer location maps. The surface flow structure plots were made by plotting the gridded and filtered median flow vector, with color shading to show the magnitude of the flow velocity. The quality of these plots was affected by the conditions in which the data was gathered. The lighting of the flume was particularly important, because it was required to light the particles as much as possible without lighting other objects that may have caused erroneous vectors to be identified. The lighting could however not be perfect in reality.

The lighting in the experiments resulted in flow vectors that were not be detected or were wrongly detected in the several parts of the flume, causing spots with very little vectors or spots with erroneous vectors. The spots with very little vectors were probably caused by the reflection of a lamp. Because in nearly all flow conditions the area (x,y)=([6.4 6.7],[3.3 4.1]) had bad and/or little data and this resulted in the fact that the grid cells in this area were filtered out. Outside of this area, in the rest of the flume, small waves could cause reflections that led to aliasing and thus led to spurious vectors or no vectors at all. Predominantly the high Froude number conditions were affected by this problem and thus the results from the high Froude number conditions were harder to interpret. Most erroneous vectors were deleted by the aforementioned filter step using the thresholds on the number of vectors and the standard error of each grid cell.

In order to detect the location of the shear layer the surface flow vorticity should be calculated using the following equation:

$$\vec{\omega} = \frac{\partial v_y}{\partial x} - \frac{\partial v_x}{\partial y} \quad (4)$$

This equation essentially calculates the flow velocity gradient perpendicular to the flow. This gradient causes shear forces in the flow and thus vortices. The curvilinear LSPIV data structure however prevented the use of this exact equation, so a slightly different vorticity-calculation was used:

[fxU, **fyU**] = gradient (Ut, g.X, g.Y);
[**fxV**, fyV] = gradient (Vt, g.X, g.Y); (5)
O = **fxV** - **fyU**;

In this Matlab script Ut and Vt were the median vector components of each grid cell, g.X and g.Y were the x and y coordinates of the gridline intersections of curvilinear grid. **fxV** = $\frac{\partial V}{\partial x}$, **fyU** = $\frac{\partial U}{\partial y}$ and O = $\vec{\omega}$, thus calculating the vorticity according to equation 4. The result of the use of this calculation method was that the vorticity values in the straight section was good, but in the bends the vorticity values are unreliable. The area of interest was in the straight section just downstream of the bend, so it did not result in problems during the analysis.

Areas with high vorticity were identified as shear layers, these areas were simplified to a single line and plotted in a separate plot. So, in these simplified shear layer plots the line indicates the time-averaged location of the shear layer where it was detectable. Some plots however indicate that there were more than one shear layer near the inner bend bank, but that was not the case. For a certain flow condition the bend was filmed at multiple camera positions and the pumps were mostly shut off while moving the camera to a new position. After restarting the pumps the equilibrium in the flume might have been slightly different than before and thus the shear layer seemed to shift between camera positions in the same flow condition. So the multiple shear layers in the vorticity plots were not happening simultaneously. But because the vorticity plots are time averaged and include every camera position for that flow condition it seems to happen simultaneously.

The maps of measured surface flow structure, maps of calculated vorticity and deduced simplified shear layer location maps are time-averaged, therefore time stack plots were made to analyze the movement of the shear layer in time. A particular cross section was chosen to analyze the shear layer movement on. Only between y=4.3m and y=4.6 m the shear layers of all flow conditions could be correctly analyzed.

Figure 10 shows an example of the time dependent plots of one flow condition, the intermediate flow depth low Froude number flow condition is shown. The first of the three plots, located at the left side in this ensemble plot, is the time stack of streamwise surface flow velocity plot. This time stack plot was made in the following steps:

- A line with these coordinates (6.050, 4.300) (6.600, 4.575) was given a width that was variable between flow conditions. For all slow conditions 25 cm was used and for the fast conditions 35 cm except for the fast deep condition, in this case 50 cm was required.

- The polygon that was defined in the previous step was divided up in 200 equally large rectangular areas;
- All vectors in the polygon were separated into small time steps of 1/15 second and separated into the 200 rectangular areas (x-position);
- An overlap in x-position and in time was specified to provide a good balance between quality and quantity of the data and thus the clarity of the picture;
    - In all cases the overlap in the x-direction was 7.5 pixels, so the value in a pixel is the mean of the nearest 7.5 pixels (23 mm) in the x-direction;
    - In the fast flow conditions the overlap in time was 20 pixels, so the value in a pixel was the mean of the nearest 20 pixels (20/15Hz = 1.33 seconds) in the t-direction. In the slow conditions the overlap is 4 pixels (0.27 seconds), except for the shallow slow condition, here an overlap of 8 (0.53 seconds) pixels was used.

The width of the polygon and the overlap in time and x-position was balanced to get the highest data quality without fading the contrast by having a too large quantity of data or resulting in blank spots by having a loo low quantity of data.

The second of the three plots, located at the top right in this ensemble plot, provides the time averaged streamwise surface flow velocity in the aforementioned polygon. This plot was used to identify the time-averaged location of the shear layer and the corresponding streamwise flow velocity. The 25, 50 and 75 percentile values were plotted to visualize the quality of the data.

The third of the three plots, located at the bottom right in this ensemble plot, shows a visualization of the movement of the shear layer in time. This plot was created by defining at what location the sudden increase in streamwise velocity, in the second plot, lay for each time step.

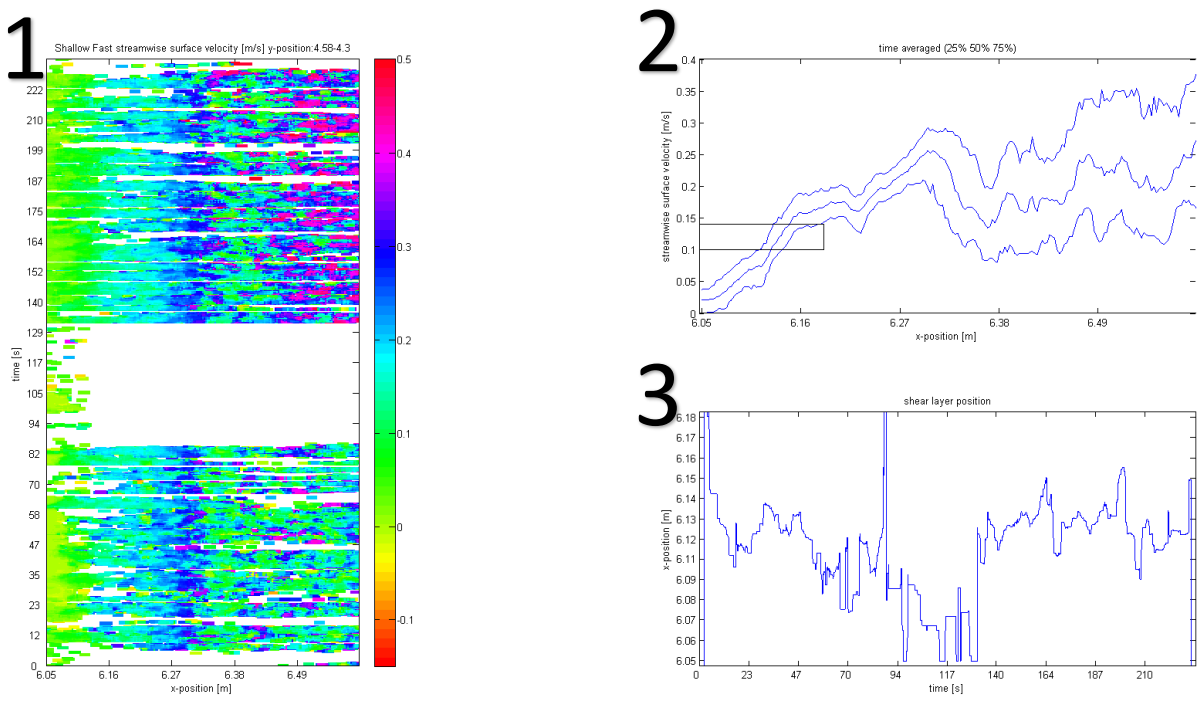

Figure 10, Example of the time stack plots of one flow conditions

4 Results

Figure 11 shows an overview of the available and significant data concerning flow separation in the first bend. In the second bend the same information is available, excluding the shear layer location plots and time dependent plots. The data will be used, step by step, to analyze flow separation in the experimental bend flow. The data will also be compared with literature, which is mentioned in the review.

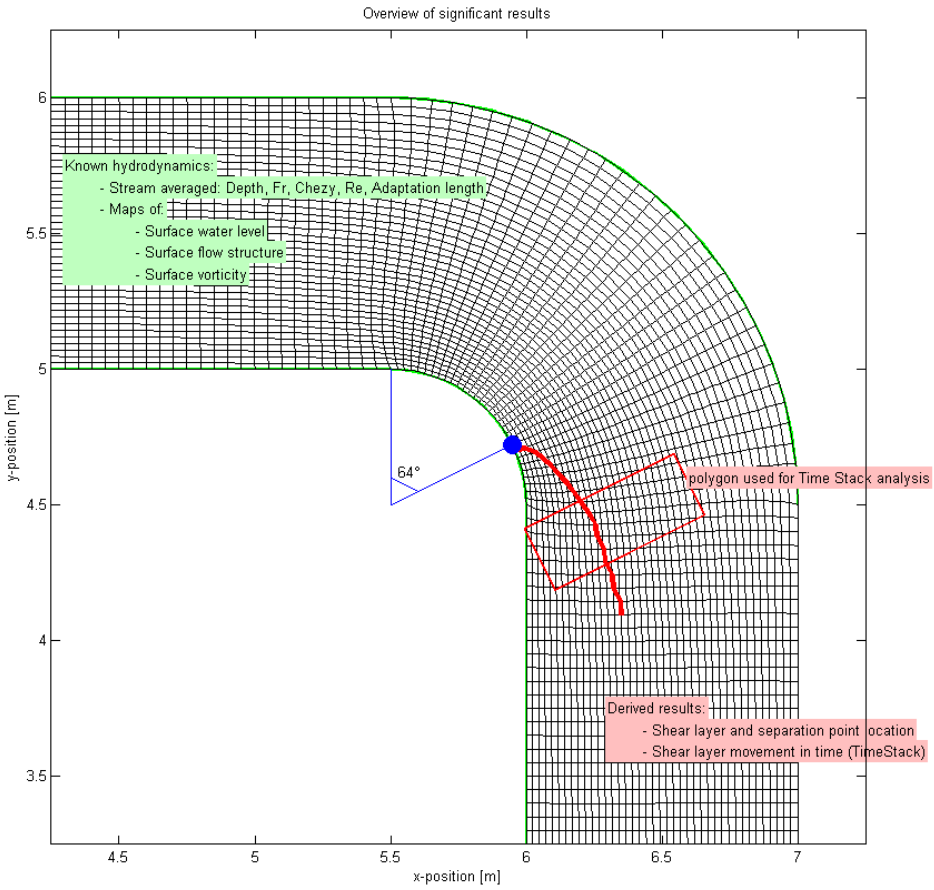

Figure 11, Overview of the significant measured and calculated data that are needed to analyze Flow Separation in the first bend

4.1 Water level

Near the inner bank the cause of flow separation typically is an adverse pressure gradient. The adverse pressure gradient is typically caused by the sudden vanishing of the curvature-induced transverse tilting of the water surface. To assess whether this is the case in the experimental results the water level measurements were analysed. Figure 12 shows the maps of interpolated water level data of three different flow conditions.

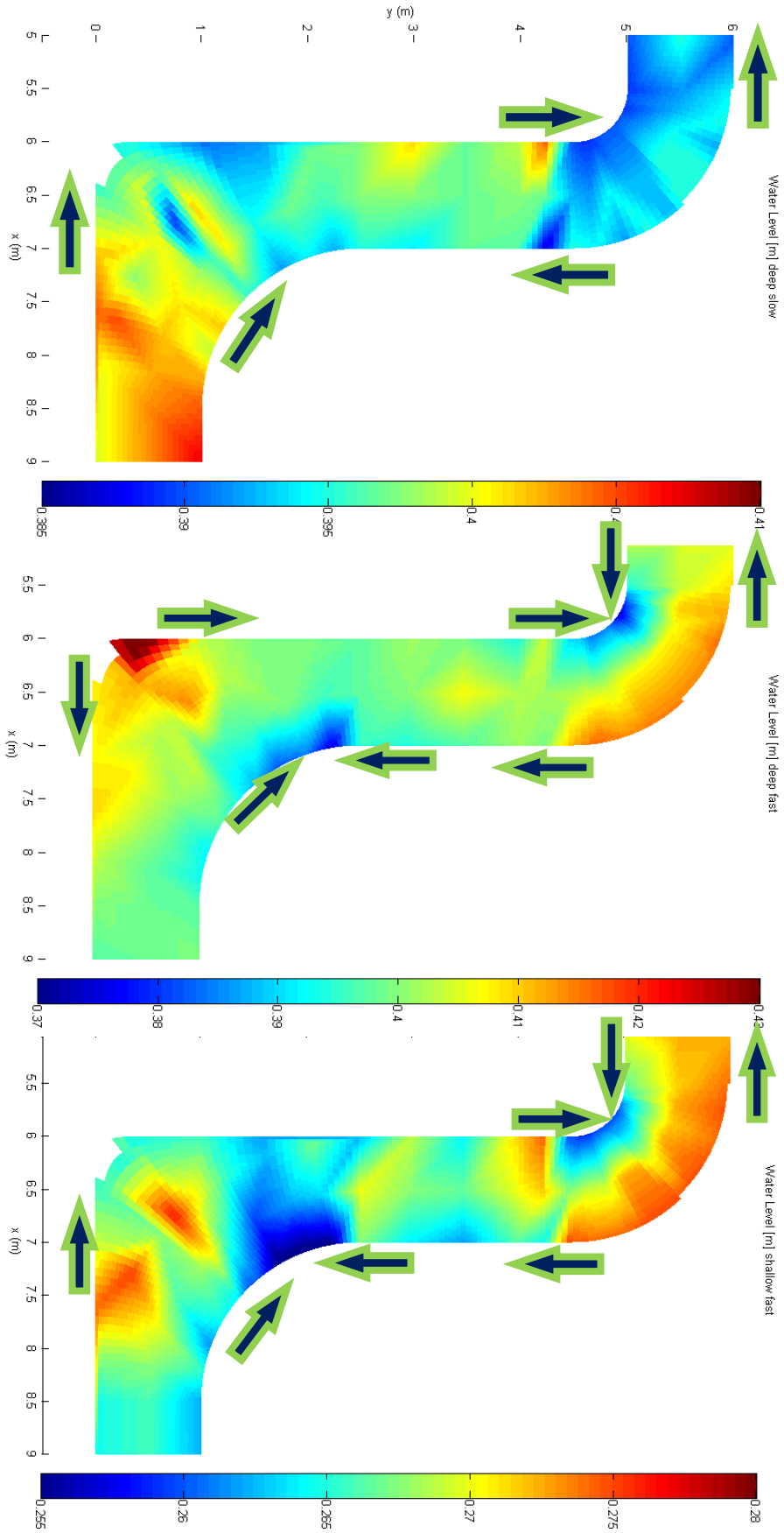

Figure 12, Interpolated water level [m], the arrows indicate a downward water surface slope.

The lower plot in Figure 12 shows the water level plot of the shallow, high Froude number condition. In this figure the transverse tilt is clearly visible in the first bend, with a drop in water level near the inner bank and a rise near the outer bank. The approximate water level difference between outer and inner bank is 15 mm, this is 19% of the average flow depth. The appearance and the vanishing of this transverse tilting leads to specific pressure gradients, indicated by the arrows. The arrows indicate a downward water surface slope. At the bend exit the transverse tilt vanishes after overshooting in the other direction. The overshoot causes a strong streamwise pressure gradient near the outer bank that accelerates the flow. Near the inner bank a sharp pressure increase, of approximately 15 mm water pressure, is formed. This adverse pressure gradient decelerates the flow and the main streamwise flow is forced to move around this stagnant water, thus causing flow separation. If the kinetic energy of the water in this area is too low to overcome the adverse pressure gradient the flow is reversed, causing flow recirculation. So the analysis of the balance between kinetic energy and the adverse pressure gradient near the inner bank is an important method for flow separation analysis.

Near the bend entrance of the outer bank a sudden increase in the transverse tilting of the water surface can cause an adverse pressure gradient. In the shallow, high Froude number condition a 2.5 mm adverse gradient can be observed at this location. The flow in the outer bank boundary layer can therefore be decelerated in addition to the deceleration caused by roughness-induced friction. The kinetic energy input in the outer bank zone is relatively large compared to the inner bank zone due to the inertia-induced impinging of the main flow on the outer bank. The smaller adverse pressure gradient near the outer bend entrance is therefore less likely to be large enough to cause flow separation, it can however cause an outer bank cell structure to occur. Only in the high Froude number, deep flow depth condition an increase in water level near the outer bank bend entrance can be observed that is likely to cause significant flow retardation. But the outer bank cell was observed in all fixed bed Hydralab III experiments (Blanckaert et al., 2012).

Table 3, Surface water level gradients in the first bend of three different flow conditions

Flow condition		Depth (m)	Froude nr. (-)	Transverse water level gradient	Adverse gradient inner bend exit	Adverse gradient outer bend entrance
Small depth	**high Fr**	0.08	0.53	15 mm, 0.86°	15 mm	2.5 mm
Large depth	**high Fr**	0.20	0.50	35 mm, 2.0°	20 mm	10 mm
Large depth	**low Fr**	0.20	0.16	± 3.5 mm, 0.20°	15 mm	± 2.5 mm

The results of the water level data analysis of all three available flow conditions is shown above, in Table 3. An increase in Froude number leads to a steeper transverse water level gradient. An increase in Froude number from 0.16 to 0.50 leads to a tenfold increase in transverse gradient. Also an increase in flow depth leads to an increase in the transverse water level gradient. A multiplication of the flow depth by 2.5 (an increase from 8 cm to 20 cm) leads to approximately the same proportional increase in the transverse tilt.

The transverse water level tilt causes the adverse gradient near the inner bend exit. However the adverse pressure gradient at this location is constant in all conditions, independent of Froude number and flow depth.

The second bend is less sharp than the first bend and has outer bank widening. These facts cause a less abrupt streamwise change in B/R, halfway the bend the same value is reached however. The value of H/B is overall smaller in the second bend and changes gradually due to the outer bank widening. According to equation (2) less transverse tilting of the water level can be expected. So also less chance of flow separation is to be expected.

In the second bend a transverse water level gradient was only observed in the deep fast flow condition. In this case the transverse water level gradient was 1.2°. Mostly all locations of downward water surface slope do not show a trend between flow conditions. Only halfway the inner bend a consistent adverse pressure gradient can be observed. In Table 4 the extent of the adverse gradients is mentioned. It can be seen that the deep fast flow condition show the greatest adverse pressure gradient in the second bend. This fact complies with the previous mentioned observed correlation of Froude number and flow depth with the adverse pressure gradients in the first bend.

Table 4, Surface water level gradients in the second bend of three different flow conditions

Flow condition		Depth (m)	Froude nr. (-)	Transverse water level gradient	Adverse gradient halfway inner bend
Small depth	**high Fr**	0.08	0.53	-	8 mm
Large depth	**high Fr**	0.20	0.50	40 mm, 1.2°	18 mm
Large depth	**low Fr**	0.20	0.16	-	9 mm

In the high Froude number conditions a greater streamwise downward water surface slope than the average cross sectional slope is observed near the entrance of the second bend. The exact cause for this fact is not certain. It could be caused by the fact that high Froude number flow causes different flow remnants from the first bend to influence the flow structures in the second bend.

The effect of the outer bend widening on the water level is uncertain, because the water level data in the second bend near the outer bank differs too much between the flow conditions.

4.2 Surface flow structure

The LSPIV analysis resulted in maps of measured, time-averaged surface flow structure. The plots are vector flow fields with colors indicating flow velocity in meters per second. In the appendix 9.2 the plots from all six flow conditions are situated side by side. Note that the colorbar values differ between the low Froude plots on the left and the high Froude plots on the right. Vector length also indicates flow velocity and the scale also differs between left and right.

Figure 13 shows two examples of the surface flow structure plots. These particular plots do not suffer from bad data quality as much as the other plots do and it clearly shows many bend flow effects. These effects will be analyzed step by step to assess what processes influence flow separation.

- Helical flow
- Contraction of the main surface flow
- A shear layer
- Downstream decreasing transverse gradients in the streamwise flow velocity
- Slight flow recirculation
- A drop in flow velocity near the outer bank

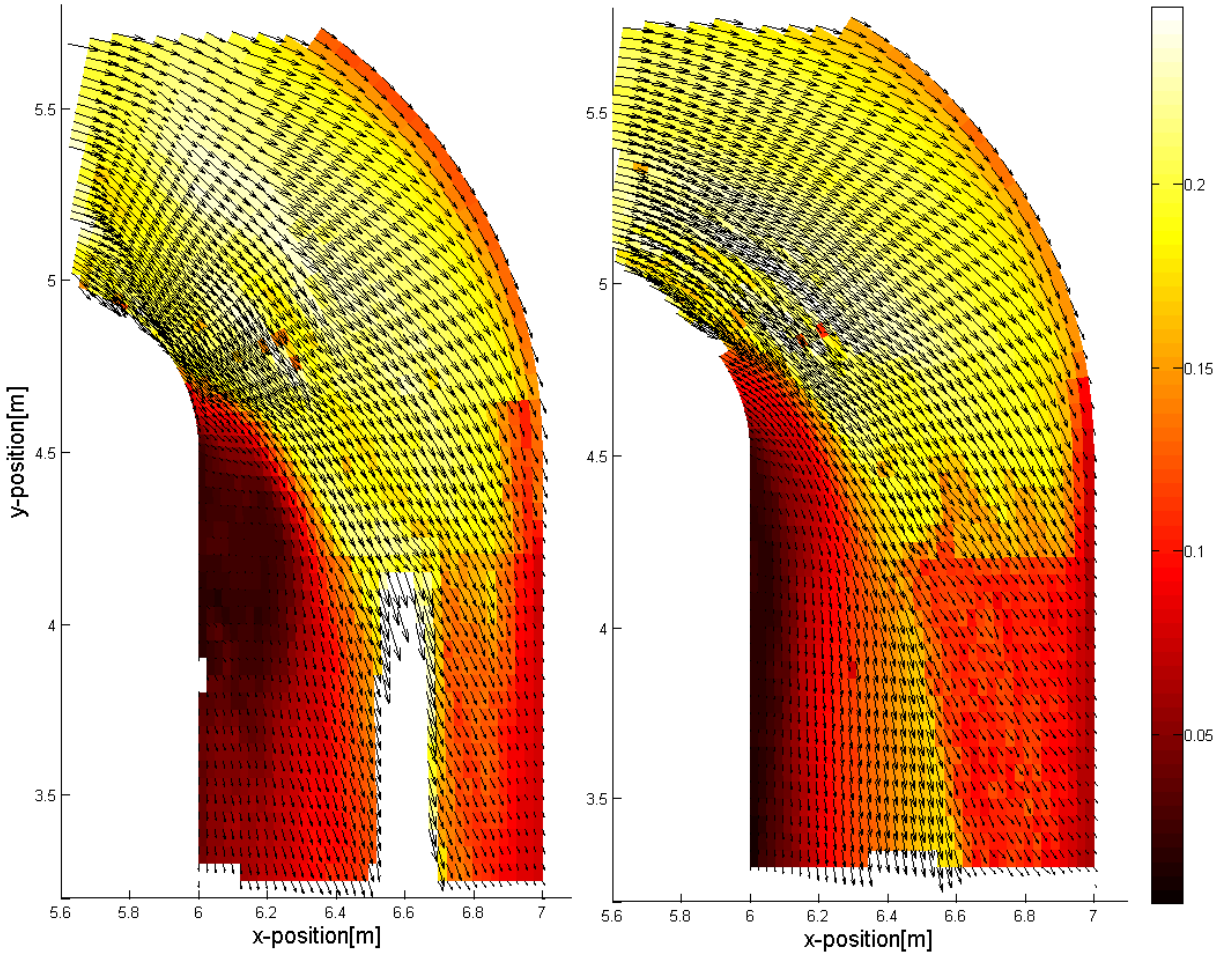

Figure 13, Time-averaged surface flow structure, vector length and color indicates flow velocity in [ms^{-1}]. The intermediate depth, low Froude condition on the left and on the right the shallow depth, low Froude.

To ascertain whether helical flow plays a role in the experiments, the surface flow structure plots (Appendix 9.2) were analyzed using the relevant meander bend processes in Figure 3.

The processes that indicate helical flow in Figure 3 are:

- A transverse water surface gradient
- Transverse surface velocity directed towards the outer bank
- The core of high streamwise velocity located near the outer bank
- Downwelling near outer bank and upwelling near inner bank

In addition to causing adverse streamwise pressure gradients in bends, the transverse water surface tilt also drives the helical flow structure together with the inertia-induced centrifugal force. So the transverse water surface gradient is an important process to look out for in order to analyze helical flow. As stated before, a transverse water surface gradient was clearly occurring in all flow conditions. In Figure 13 it can be seen that the core of high surface flow velocity outside the separated zone is directed towards the outer bank. And the core of high surface flow velocity is located near the outer bank. Flow vectors that do not align with the flume wall indicate that upwelling or downwelling is occurring. Downwelling seems to be more pronounced near the outer bank in the high Froude number flow conditions. In all flow conditions (Appendix 9.2) the four processes mentioned above can be observed. Also in the ADVP measurements helical flow was unmistakably observed (Blanckaert et al., 2012). So helical flow is occurring in all flow conditions.

In Figure 5 Bridges & Leeder (1976) have sketched the main characteristics of flow separation, it can be seen that the main flow is contracted, the shear layer moves away from the bank and creates spiral vortices that decay in the downstream direction. These processes will be discussed below, because they also play a role in the surface structure plots.

The surface flow structure plots of all flow conditions show a clear and sharp transition in the streamwise flow velocity just downstream of the bend apex. So in all flow conditions a shear layer is present. Closed separated zones and flow recirculation were observed in the mobile bed experiments, in all fixed bed flow conditions an open separated zone is observed (Blanckaert et al., 2012). Indicating that probably flow recirculation does not play a great role in the data-sets analyzed in this report. To assess whether this is true, zoomed in plots of the separated zone were plotted. These plots are situated in Appendi 9.3. The colors on the colorbar are inverted and the vector length of the unzoomed plots is multiplied by six to focus on the low velocity flow structures in the separated zone.

In most surface flow structure plots of the separated zone the vectors are too irregular for proper analysis. Or blank spots inhibit the analysis of the separated zone. In the low Froude, shallow and intermediate depth conditions (Figure 14) the clearest flow structure is found. In the intermediate depth, low Froude condition (left plot) clear zones of reversed flow are observable, but not recirculation. This is indicated by the blue arrow. Similar structures of reversed flow are expected in the other flow conditions.

The blue arrows in the shallow depth, low Froude condition plot indicate a small closed recirculation zone inside the open separated zone. The flow velocity in this zone is however so small that the recirculation can be assumed to be insignificant. So, the weak upstream currents in the separated zone downstream of the bend apex are not significant in the fixed bed experiments.

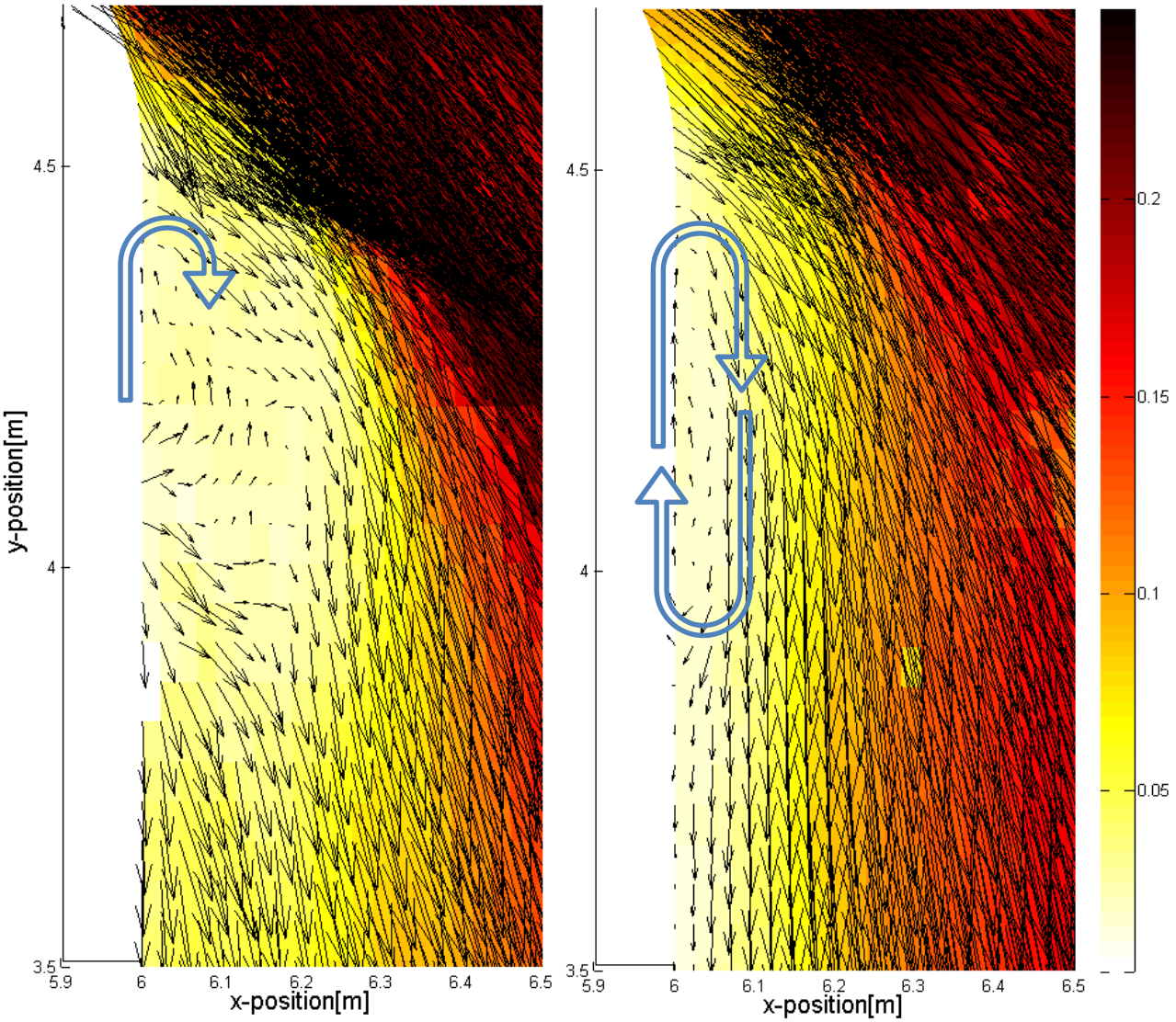

Figure 14, Surface flow in the separated zone, vector length and color indicates flow velocity in [ms^{-1}]. Flow reversal and recirculation is indicated by the blue arrows. The intermediate depth, low Froude condition on the left and on the right the shallow depth, low Froude.

Near the inner bank the surface recirculation typically has a vertical axis of rotation, which can be confirmed by the flow structures in Figure 14. The structure of the recirculation below the surface can however not be analyzed using the LSPIV data. Near the outer bank flow recirculation has a horizontal and streamwise axis of rotation, spinning in the opposite direction of helical flow. The outer bank cell is caused by the friction-induced drop in flow velocity near the outer bank and it may result in small vortices. The presence of an outer-bank cell widens the outer-bank boundary layer by repelling maximum streamwise velocities towards the inner edge of the outer-bank cell (Blanckaert et al., 2012).

In all experimental flow conditions, except the intermediate depth, high Froude condition the flow velocity near the outer bend bank is lower than the main flow. This may indicate the existence of an outer bank cell. However, the surface flow near the outer bank in all flow conditions is not directed towards the inner bank, which would be likely in the case of an outer bank cell. And because only the surface flow structure is known and not the 3D flow, the existence of the outer bank cell cannot be confirmed in any flow condition.

To ascertain whether helical flow plays a role in the second bend, the surface flow structure plots (Appendi 9.4) were analyzed in the same way as was done for the first bend. In the second bend only in one flow condition a clear transverse water surface gradient was observed.

Near the second bend entrance the core of high surface flow velocity is located near the inner bank, this is not the case in the first bend. Also the surface flow is not directed towards the outer bank in the first halve of the bend, which is the case in the first bend. It can thus be stated that these differences are caused by flow structure remnants from the first bend. In the second halve of the second bend the flow is directed towards the outer bank, which implies that helical flow is occurring. This can be confirmed by the fact that the vectors near the inner and outer bank near the end of the second bend do not perfectly align with the bank. This implies that slight downwelling is occurring near the outer bank and slight upwelling is occurring near the inner bank.

The flow velocity near the outer bank is very low compared to the flow velocity of the main flow, this is the case in all flow conditions. This implies that this section of the flume is separated. However, no sharp transition in the streamwise flow velocity can be observed near the second bend outer bank entrance. The flow separation with no clear shear layer is likely to be caused by the outer bank widening.

The separated zone recirculates with a vertical axis of rotation. Zoomed in plots of the recirculation zone in the second bend are located in the appendix 9.5. Figure 15 shows the surface flow in the separated zone of the second bend of the intermediate depth low Froude flow condition. The main flow separates from the outer bank at approximately (x,y)=(6.0, 1.3) and reattaches at approximately (x,y)=(7.2, 0.0), indicated by the red dots.

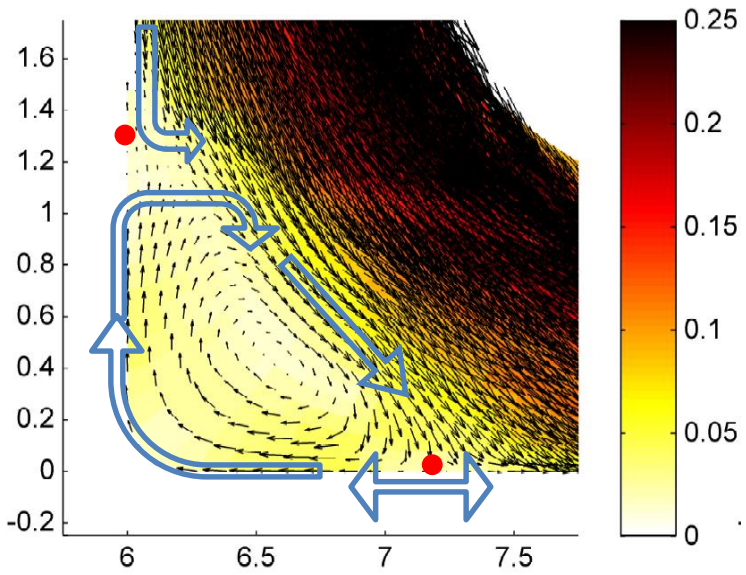

Figure 15, Surface flow in the separated zone of the second bend of the intermediate depth low Froude condition. Vector length and color indicates flow velocity in [ms^{-1}], flow recirculation is indicated by the blue arrows and the separation and reattachment point is indicated by the red dots.

The separation- and reattachment points of the outer bend separation zone were analyzed for all flow conditions and are shown in Table 5. The location of the separation- and reattachment points were the comparable for same flow depth conditions, so the location of separation and reattachment is not dependent on Froude number. The extent of the outer bend separated zone shows a clear correlation with the flow depth. So, flow depth has a negative effect on the extent of the separated zone.

Table 5, Separation- and reattachment points of the outer bend separation zone.

Flow condition	Depth (m)	Separation point (x,y)	Reattachment point (x,y)
Small depth	0.08	(6.0, 1.7)	(7.4, 0.0)
Intermediate depth	0.14	(6.0, 1.5)	(7.2, 0.0)
Large depth	0.20	(6.0, 1.3)	(7.1, 0.0)

The separated flow near the outer bank does not contribute to the main flow, so the core of high surface flow velocity is located near the approximate comparable location as in the first bend. This fact in combination with the fact that an adverse pressure gradient was observed in three flow conditions halfway the inner bank makes it possible for flow separation to occur downstream of the inner bend apex. However, only the shallow flow conditions and the intermediate depth slow flow condition show a sharp transition in the streamwise flow velocity just downstream of the bend apex.

4.3 Surface vorticity

Blanckaert (2011) states that the sharp transition in velocity, in the horizontal bed experiment, was found to coincide with the location of the vertical spiral vortices that indicate the existence of a shear layer. So the shear layer at the edge of the separation zone is characterized by a core of positive vorticity (Blanckaert, 2011). Plotting vorticity can thus help to identify the location of the shear layer consistently and it can help to analyze its dependence on flow depth and Froude number.

The surface vorticity plots are calculated using equation [**fxV**, fyV] = gradient (Vt, g.X, g.Y); (5) mentioned in the methods. The resulting plots (Appendix 9.6) indicate the time averaged extent of spinning motion per grid cell in [s^{-1}] with color shading. The high Froude number conditions show a messy distribution of vorticity and blank spots, making it hard to analyze. This messy picture can be caused by a more turbulent flow or reflections due to waves. In this case the shear layer can be identified, but with less certainty than in the low Froude number conditions.

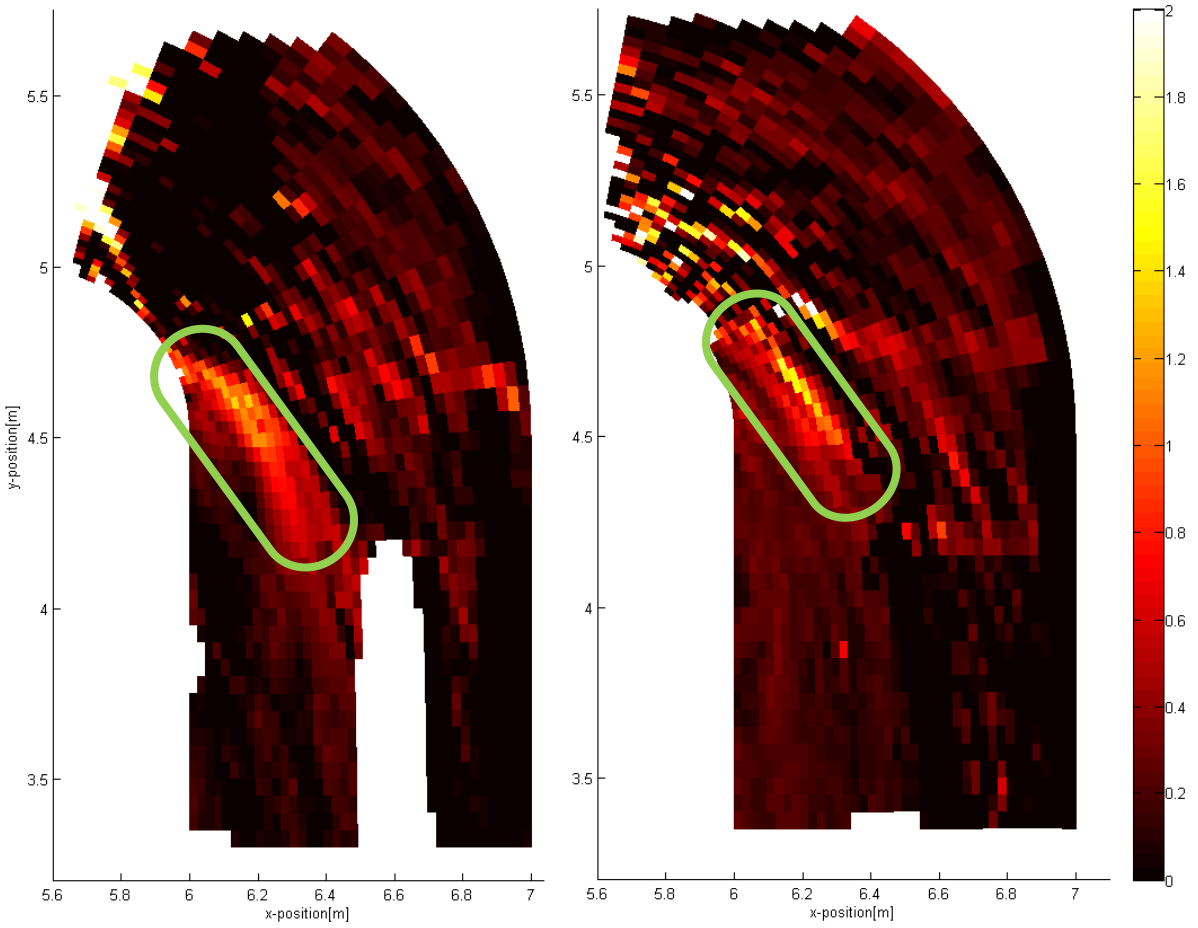

Figure 16, Surface vorticity [s^{-1}] indicated by color. The green contours lines indicate areas with high voriticy associated with the shear layer location. The intermediate depth, low Froude condition on the left and on the right the shallow depth, low Froude.

Figure 16 shows the surface vorticity of the intermediate depth, low Froude and the shallow depth, low Froude conditions. These are same flow conditions as in Figure 13 and Figure 14, in these conditions the clearest vorticity structure is found. The shear layer can be identified by the areas with a vorticity higher than 1 s^{-1}, roughly indicated by the green contours. The viscosity-induced downstream decreasing transverse gradient causes the vorticity to decrease in the downstream direction, so the shear line stops after a certain distance.

In all other flow conditions the shear layers starts at the inner bend bank and dissipates into the main flow approximately 50 to 100 centimeters downstream. And the overall extent of vorticity is approximately the same in all conditions and are roughly the same in the main flow as in the separated zone.

The vorticity plots of the second bend are located in appendix 9.7. The plots of the shallow flow conditions show a clear shear layers starting halfway the inner bank near the adverse pressure gradient. No shear layers can be observed near the inner bank in the other flow conditions. No clear shear layer can be observed that separates the outer bank recirculation cell from the main flow. A shear layer near this location is expected due to the fact that the main flow velocity is significantly higher than the separated flow.

4.4 Shear layer location

To clarify the location of the shear layer in the first bend in all six flow conditions, data reduction was performed. This was done by identifying the shear layers, as stated in the previous paragraph, and by plotting one single line of maximum vorticity per flow condition. The resulting shear layer locations can be seen in the shear layer location plots below, Figure 17 shows the shear lines divided by Froude number and Figure 19 shows the shear lines divided by flow depth.

It should be noted that because the high Froude number conditions resulted in low quality maps of vorticity the resulting simplified shear lines of these flow conditions are also of fairly low quality. Therefor the shear layer length cannot be assessed and analyzed. The blue line in all subplots in Figure 17 and Figure 19 indicates the cross section that is used to analyze the transverse location and the temporal variation of the shear layers in all flow conditions. These analysis steps will be discussed below.

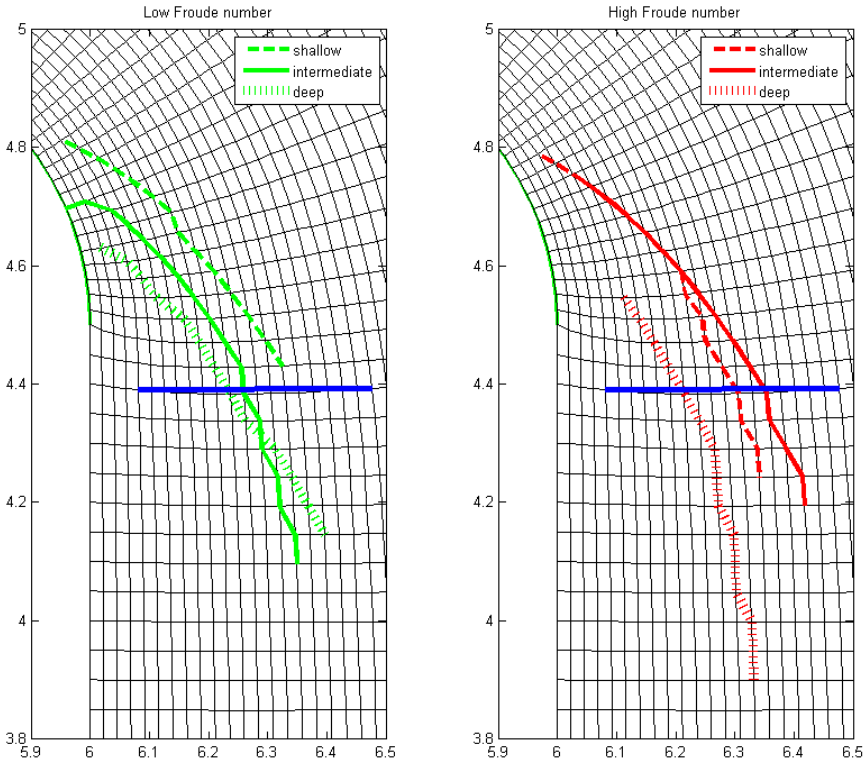

Figure 17, Shear layer locations for different Froude numbers

In Figure 17 the flow depth shows a relation with the surface location of the shear layer, the deeper the flow the further downstream and towards the inner bank it moves. This coincides with the expectations. The downstream shift of the shear layer in deeper flow can thus be correlated to the adaptation length. However the downstream shift of the shear layer between the different flow depths is much smaller than the adaptation length calculation suggests. The movement towards the inner bank is inherent to the downstream movement, because the shear layer moves away from the inner bank while moving downstream.

The shear layer in the intermediate depth, high Froude number condition is further upstream from the smaller water depth, high Froude number condition. So this flow condition does not show the aforementioned relation. When only considering the more reliable low Froude conditions the hypothesis stands.

To visualize the location of the shear layer and its dependence on flow depth the distance from the bank versus the flow depth is plotted in figure 18. The blue line in figure 17 and 19 (y=4.39m) is used as a cross section to analyze the location of the shear layers just downstream of the bend for all flow conditions. This particular cross section is used, because only on this line the shear layer location can be determined for all flow conditions.

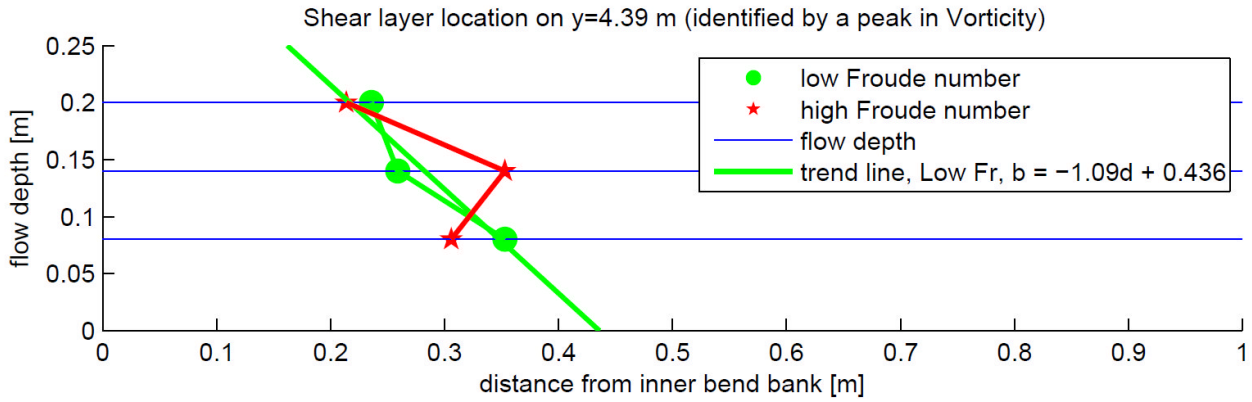

Figure 18, Transverse shear layer location on a cross-section 11 cm downstream of the first bend exit (y=4.39).

In figure 18 the high Froude number flow conditions do not show a clear trend, this is likely caused by the low quality of the data. When the intermediate depth, high Froude number condition is not considered a similar trend as in the low Froude conditions can be observed. The low Froude number flow conditions show a clear trend between flow depth and distance from inner bend bank with a coefficient of determination (R^2) of 0.89. The deduced formula of the trend line is:

$$b = -1.09d + 0.436 \quad (6)$$

Where b is the distance [m] of the shear layer from the inner bend bank and d is the flow depth [m]. The relation of flow depth and the distance from the bank in this plot is influenced by the location of the separation point, because the downstream movement of the shear layer goes along with the movement away from the bank. The relation between the distance from the bank and flow depth is thus indirect.

The previous findings suggest that an increase in flow depth causes a downstream movement of the shear layer and thus a movement of the shear layer towards the bank at a fixed cross section. In figure 18 this relation is clearly visible, in the cross section of the flume the shear layer moves towards the inner bank with increasing flow depth.

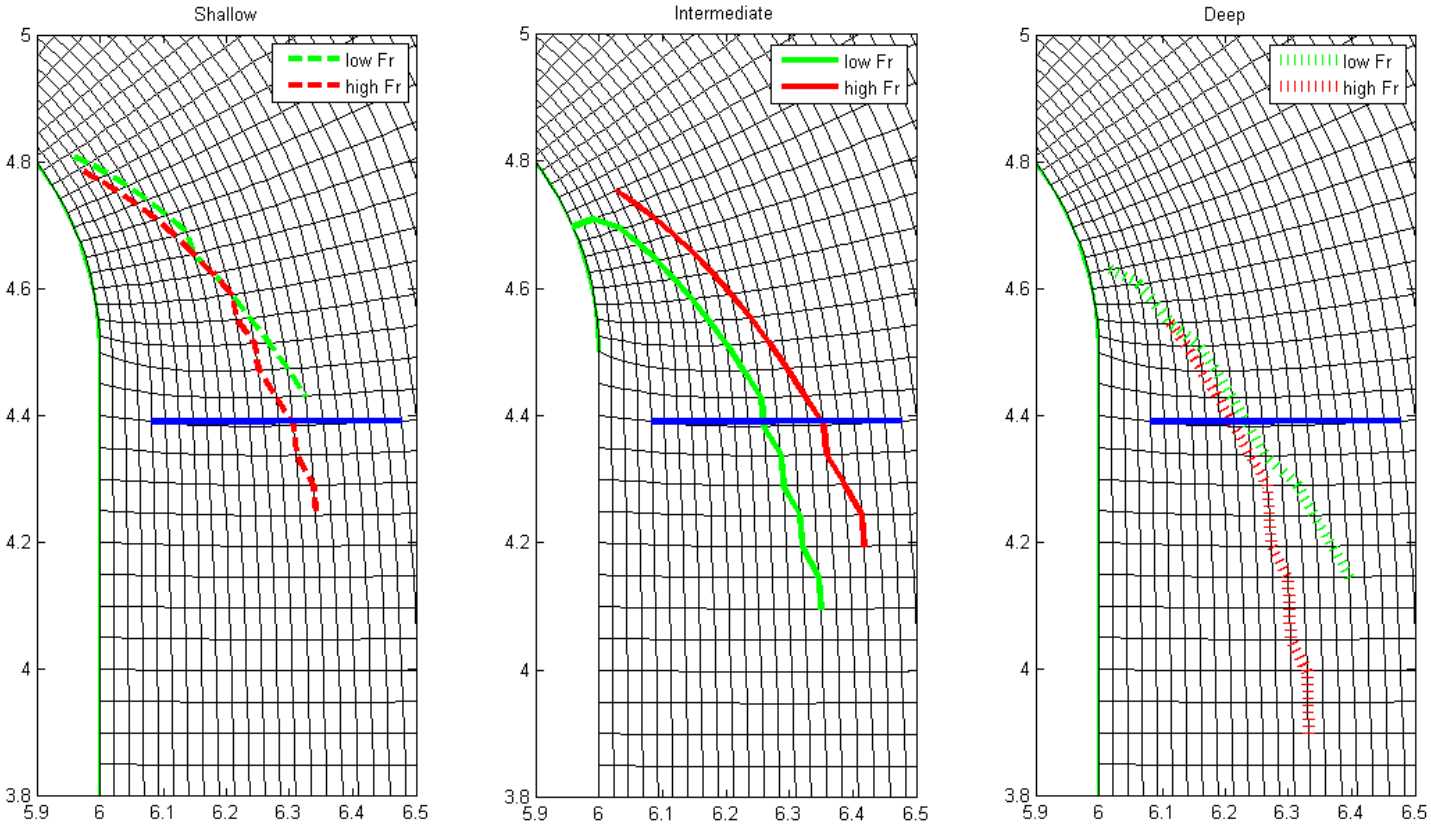

Figure 19, Shear layer location for different flow depths (8, 14 and 20 cm)

In the shallow and deep flow conditions, in figure 19, the shear layer is located further downstream in the higher Froude number flow. However, the intermediate depth, high Froude number condition does not show this relation. This is the same flow condition that does not fit the relation of flow depth with the shear layer location, described in the previous paragraph. Indicating that this particular flow condition might be erroneous.

The start of the known part of the high Froude number shear layers of the shallow and deep flow conditions in figure 19 are located at the same location as the low Froude number shear layers. Indicating that the separation point does not depend on the Froude number. The exact separation point of the low Froude number conditions will be discussed in the next section.

The end of the shear layer, in the deep and shallow flow conditions, bends towards the inner bank with increasing Froude number. The higher kinetic energy of the main flow in the high Froude number conditions pushes the end of the shear layer towards the inner bank. This process opposes flow contraction.

4.5 Separation point location

Another method to analyze the different shear lines is to look at the separation point. The separation point is the point where the velocity is zero and where the boundary layer leaves the bank (Schlichting & Gersten, 2000).

In the hydralab III experiments the location of the separation point was determined with the use of the shear layer location plots of figure 17 and 19 and reported in table 6. The separation point of the high Froude number conditions could not be determined with high certainty because of low data quality. By approximate extrapolation an area is given in table 6 where the separation point could have been.

Table 6, Location of the flow separation point derived from extrapolation of the shear layer to the inner bend bank.

	8 cm flow depth	14 cm flow depth	20 cm flow depth
Low Froude number	55° (5.91, 4.79)	64° (5.95, 4.72)	73° (5.98, 4.65)
High Froude number	51° (5.89, 4.82) to 58° (5.92, 4.76)	51° (5.89, 4.82) to 58° (5.92, 4.76)	64° (5.95, 4.72) to 81° (6.00, 4.58)

It can be seen that the separation point moves downstream with increasing flow depth. This is the same relation as was found in the analysis of flow depth and shear layer location. The flow depth shows a linear relation with the distance the separation point moves between flow conditions. In the experimental data the downstream movement is approximately 8 cm with a 6 cm increase in flow depth.

The linear relation is also found in the calculation of the adaptation length of flow (1). This equation states that the expected downstream movement of flow structures correlates with mean flow depth and friction squared. So the correlation of the downstream movement of the separation point, which is a flow structure, and the flow depth could be linked with the adaptation length of flow. According to the equation however the increase in adaptation length is 3.75 meter with a 6 cm increase in flow depth. So it is unlikely that the separation point is directly influenced by the adaptation length of flow, there could however be an indirect link.

The position of the separation point is independent of the Reynolds number. The Reynolds number increases with increasing Froude number and the location of the separation point does not depend on the Froude number. It can be concluded that the location of the separation point does not depend on the Reynolds number either.

The separation point is located upstream of the adverse pressure gradient, so upstream of the point where the transverse water surface tilting vanishes. In the deep, low Froude condition the separation point is located at (5.98, 4.65) and the adverse pressure gradient is located at (6.00, 4.35). So flow separates approximately 30 cm upstream of the adverse pressure gradient in this flow condition. The comparison of water level data and separation point can only be done for the deep, low Froude condition, because only in this flow condition the water level data and separation point location are both known. So, the flow retardation effect of the adverse pressure gradient is located approximately 1.5 times the flow depth upstream of the actual adverse pressure gradient.

4.6 Temporal variation

All previous discussed plots are time averaged. To assess the dependence of Froude number and flow depth on the temporal variation of the shear layer location three plots per flow condition were made. In these plots the transverse shift of the shear layer in time is analyzed for all flow conditions. Figure 20, Figure 21 and Figure 22 show an example of the plots of the intermediate depth, low Froude condition. In the Appendix 9.8 all temporal plots of all flow conditions are situated.

Figure 20 shows the time stack plot of the intermediate depth, low Froude flow condition. In this plot a clear and sharp transverse transition in velocity can be observed. The transition lies between x=6.23m and x=6.30m and moves between these values in time. The location of this transition coincides with the location of the shear layer in the shear layer location plots (Figure 17 and Figure 19).

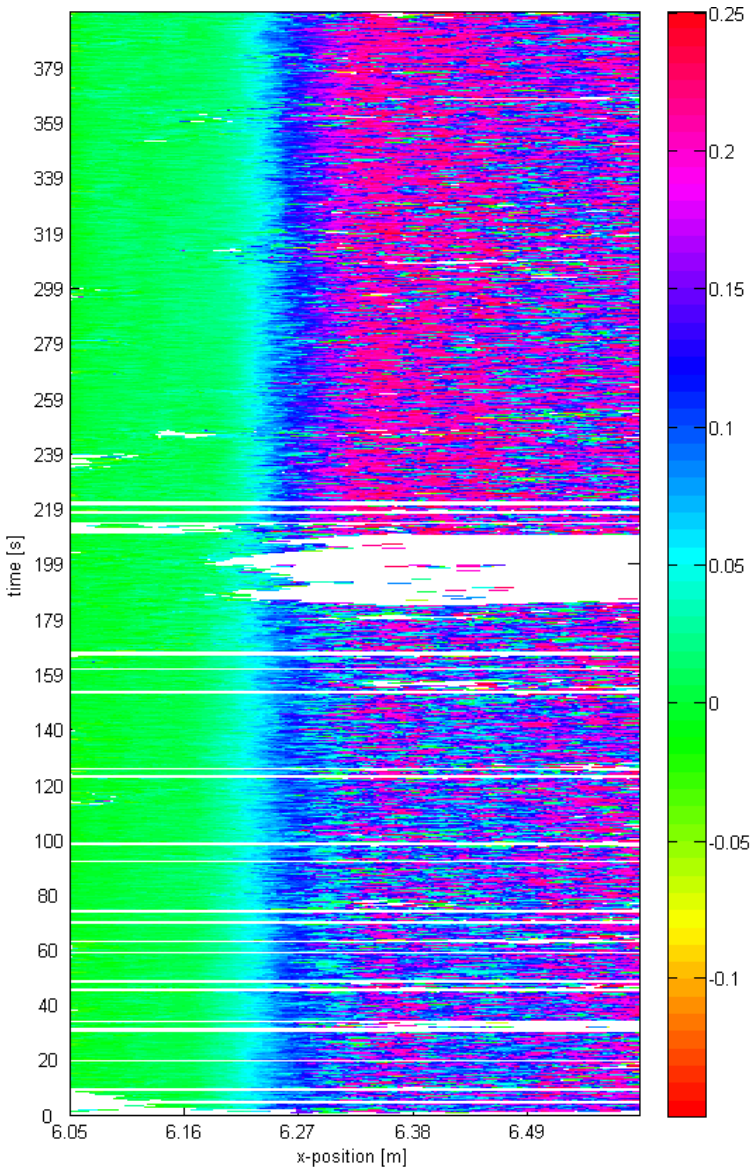

Figure 20, Time Stack of the streamwise surface flow velocity [ms^{-1}] at a cross section just downstream of the first bend exit (y=4.3m to y=4.6m) in the intermediate depth, low Froude flow condition.

The timestamps of the moments that large white spots in the timestack plots happen coincides with the start or ending of a camera position. This is caused by the fact that the seeding starts just after the camera is switched on and the camera is switched of just after the seeding stops. In the case of Figure 20 the analyzed polygon has two camera positions, one camera position from 0 to 200 seconds and from 200 to 390 seconds is the second camera position. The white area from t=180 to t=215 is thus due to little vectors in the end or beginning of a camera position. In the third graph this may lead to spikes that should not be analyzed, because they are an artifact of the data analysis.

Figure 21 provides the time averaged streamwise flow velocity in the aforementioned polygon and is essentially the average flow velocity over the x-position. In Figure 21 the time averaged location of the shear layer and the corresponding flow velocity at the shear layer can be determined. This is necessary for the next analysis step, in which the location of the shear layer at every time step is determined.

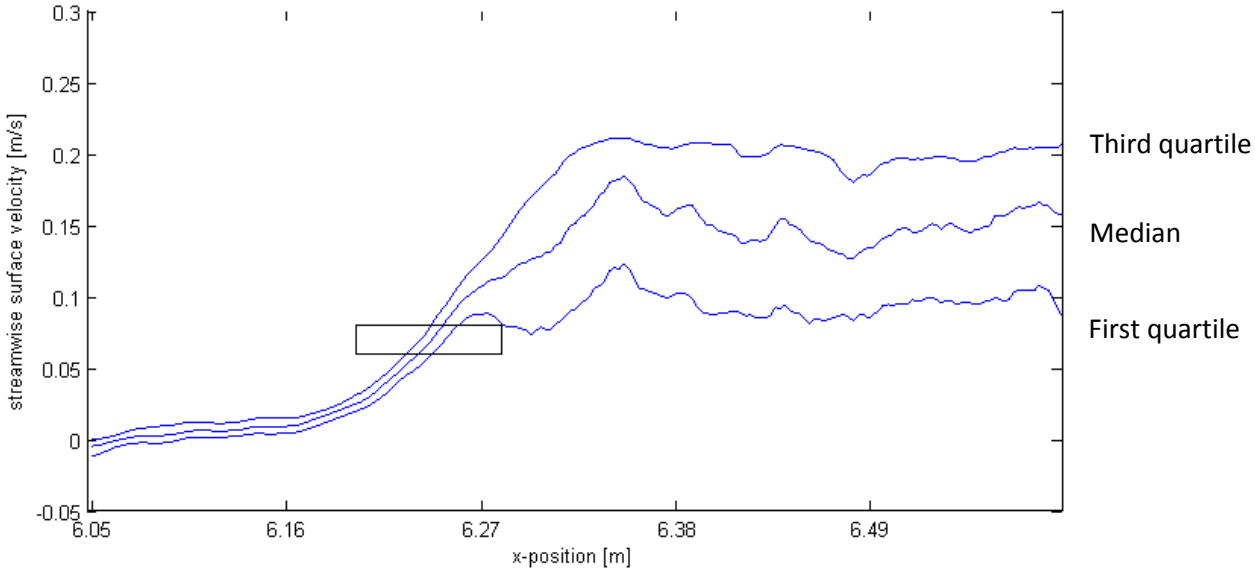

Figure 21, Time averaged surface flow velocity quartiles [ms^{-1}] at a cross section just downstream of the first bend exit (y=4.3m to y=4.6m) in the intermediate depth, low Froude flow condition.

In addition to the fact that Figure 21 is necessary to find the temporal variation in shear layer location, the plot also shows the overall variation in flow velocity with the three quartile lines. The variation between these three lines indicates the possible variation in strength, width and location of the shear layer, because the sharp transverse velocity gradient shifts with the varying transverse distribution of streamwise flow velocity.

The variation in flow velocity is much smaller in the separated zone than in than in the main flow. This can be observed in all flow conditions and is likely caused by the turbulence generated by the shear layer. The overall greater difference in flow velocity between the first and third quartile in the main flow is however also caused by the overall higher flow velocity and thus larger possible variation.

In Figure 21 the first quartile line shows that the shear layer is located at approximately x=6.24m with a 7 cm width and the third quartile line shows that the shear layer is located at x=6.27m with a 13cm width. This is indicative of the possible movement of the shear layer. The shear layer constantly "flaps" between these approximate locations and thus creates "waves" of vorticity. In this flow condition the transverse gradient is roughly constant between the quartile lines, indicating that the shear layer strength is constant.

The approximate time averaged location of the shear layer and the corresponding flow velocity were identified in Figure 21, and indicated by the black box. At every time step the location of the shear layer can be determined by searching for this flow velocity at the shear layer. The result is a plot which shows the shear layer location in time. This plot can be used to analyze the "shear layer flapping" by identifying the period and horizontal displacement of the vorticity "waves".

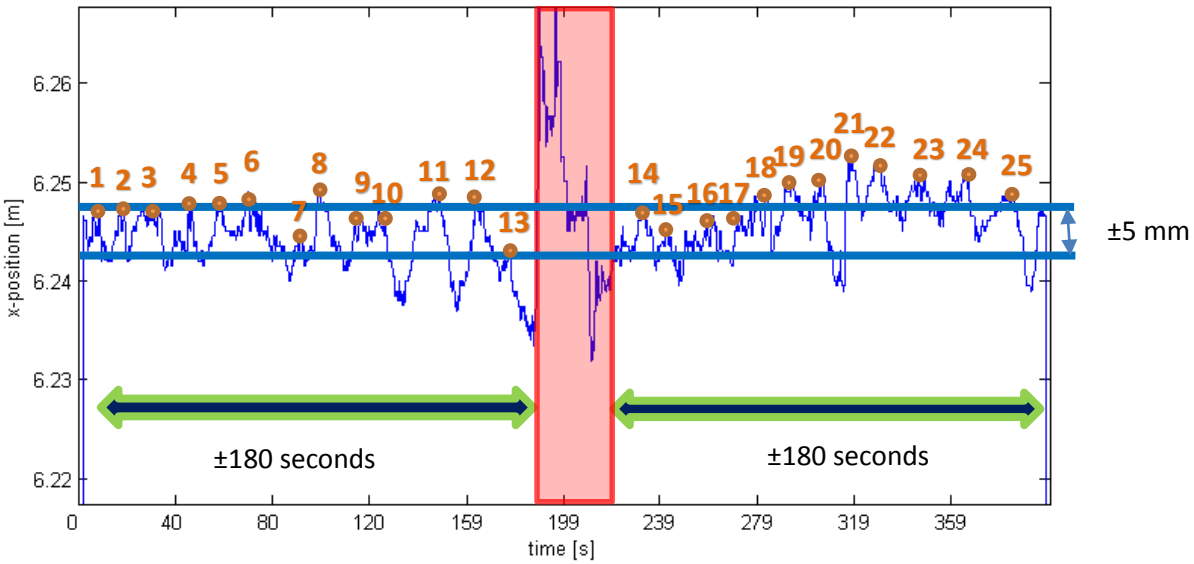

Figure 22, Shear layer location variation in time at a cross section just downstream of the first bend exit (y=4.3m to y=4.6m) in the intermediate depth, low Froude flow condition.

The spikes around t=200s, indicated with the red area, are artifacts of the data analysis method due to the transition between camera positions. So the spikes will not be analyzed. By counting the peaks and dividing the corresponding amount of time by the amount of peaks the period of the "shear layer flapping" is determined. In Figure 22 the amount of peaks is 25, indicated by the orange dots and numbers, and the corresponding time is 360 seconds. So "shear layer flapping" in the intermediate depth, low Froude condition displays a period of 360/25=14.4 seconds and a horizontal displacement range of 5 mm. The horizontal displacement range is determined by subtracting the minimum x-position from the maximum x-position, indicated with the blue lines, while excluding obvious artifacts and deviations on a longer time scale than a few waves.

The analysis method, described above, is performed for all flow conditions. The results are presented in Table 7 and Table 8. The high Froude number conditions were analyzed, but the values are of low quality. So, no definitive conclusions can be made based on the high Froude number results.

Table 7, Wave period (s) of the shear layer flapping

	8 cm flow depth	14 cm flow depth	20 cm flow depth
Low Froude number	14.2	14.4	11.2
High Froude number	11.7	14.4 – 11.9	12.2

Table 8, Horizontal displacement range (mm) of the shear layer flapping

	8 cm flow depth	14 cm flow depth	20 cm flow depth
Low Froude number	100 (uncertain)	5	10
High Froude number	25	140 (uncertain)	75

The overall average shear layer period is 13 seconds and it is rather constant between the flow conditions. No significant trends can be discovered. The overall average horizontal displacement range of the shear layers is 60 mm, which is 6% of the channel width and 43% of the average flow depth. However, the values are scattered and two values deviate too much, indicated in blue, from the average displacement range. When the uncertain values are not considered a rather clear trend can be observed, which is an increase in horizontal displacement range with an increase in flow depth and/or Froude number.

5 Discussion

The influence of flow depth (according to Blanckaert et al. (2012)), Froude number (according to Leeder & Bridges (1975)) and streamwise increase in curvature (according to Leeder & Bridges (1975), Hodskinson & Ferguson (1998), Blanckaert (2011) and Blanckaert et al. (2012)) on flow separation was also observed in the results. The second bend likely showed less consistent flow separation due to a more gentle increase in streamwise curvature. Flow depth, Froude number and streamwise increase in curvature all have a positive influence on the transverse tilt of the water level. And the transverse water level has a positive influence on the formation of flow separation.

According to Hodskinson and Ferguson (1998) the upstream channel planform is an important factor for flow separation. This was confirmed in the results. The second bend showed significantly different flow structures and a less consistent shear layer location. It should however be noted that the differences between flow structures in the first and second bend are also caused by the outer bank widening and a more gentle bend. According to Hickin (1977) the curvature needed to induce inner bank flow separation is R/B<=2. In the bends the value is never exceeded, however the value in the second bend entrance is double of that in the first bend entrance.

Blanckaert (2011) observed in experiments that the separation point was located at 40 degrees into the bend. In this report the separation point was found to be located between 55 and 73 degrees into the bend. The hydrodynamics and planform of the bend in the experiment of Blanckaert (2011) were different however. In these experiments the flow depth and Froude number are comparable to the experiments used in this report, but the flume was marginally wider, the bend slightly less sharp and the bend extended for more than 90 degrees.

Blanckaert et al. (2012) noted that remnants of helical flow structures of an upstream bend opposes the onset of inner bank flow separation and favors the generation of an outer-bank cell or flow separation. This statement can be confirmed by the findings in this report.

Flow expansion at the bend apex causes outer bank flow recirculation according to Hickin (1977), Page & Nanson (1982) and Hodskinson & Ferguson (1998). This exact relation is not confirmed in this report, it is however very likely that the outer bank flow recirculation in the second bend in the experiments is caused by the outer bank widening.

5.1 Limitations

Only flow depth, Froude number, Reynolds number and adaptation length could be discussed in the results. Because Roughness and channel planform are constant and thus their impact on flow separation could not be investigated with the Hydralab III results.

Several other parameters that have an influence on flow separation could not be tested with the Hydralab III results, because in the first bend flow separation is occurring in all flow conditions. So tests cannot be done to assess what parameters influence the onset of flow separation.

Only surface flow is analyzed with the use of the LSPIV data. This is a shortcoming, because the separation zone is not uniform over the flow depth. Blanckaert (2011) stated that experiments showed that the separation zone narrows from the water surface toward the bed and does not even extend over the entire flow depth. Indicating the importance of the analysis of 3D flow.

The flow structures in the second bend are influenced by the remnants of flow structures from the first bend. For example remnants of helical flow, flow separation and flow recirculation. It is therefore difficult to assess what the exact causes of the flow structures in the second bend are.

5.2 Recommendations

Several additional flow conditions, in which flow separation is not occurring, could have provided insight in the influence of several parameters on the onset of flow separation. For example flow conditions with a very low Froude number flow, a gentler bend or rougher boundaries.

A follow-up research that uses the results of this report to construct and calibrate a Delft3D model could provide insight in complex 3D flow structures and the internal processes that play a role in these complex 3D flow structures. It could also investigate the dependence of bend curvature and roughness on flow separation, and investigate what values of several parameters have an influence on the onset of flow separation. It could also test what the effect of the first bend is on the second bend by straightening the first bend in the model.

6 Conclusion

The conclusion of this report is partly based on the literature research that was done prior to the main analysis of the LSPIV results.

An increase in flow depth and/or Froude number both lead to an increase in transverse water level tilt in the first bend. The flow structure remnants from the first bend cause helical flow not to occur in the first halve of the second bend. In the second halve of the second bend helical flow is occurring. The transverse water level tilt (mainly in the first bend) is responsible for the fact that flow depth and Froude number both have a positive effect on the extent of helical flow in bends. The positive effect makes downwelling more pronounced near the outer bank in the high Froude number flow, this is observed in the experiments. Helical flow and flow separation both push the main flow towards the outer bank. Thus causing flow contraction and scour holes near the outer bank if the bed is mobile.

The transverse water level tilt causes an adverse pressure gradient near the inner bend exit. This adverse gradient is constant between flow conditions, independent of Froude number and flow depth. The adverse gradient retards the flow and causes flow separation. And thus the analysis of the balance between kinetic energy and the adverse pressure gradient is an important method for flow separation analysis. The flow retardation effect of the adverse pressure gradient is located approximately 1.5 times the flow depth upstream of the actual adverse pressure gradient.

The results of all flow conditions show a clear shear layer with a sharp transition in flow velocity. Not in the second bend however. The sharp transition in flow velocity in the first bend causes vorticity. All shear layers end 50 to 100 cm downstream of the separation point, so all flow conditions show an open separated zone. No significant flow recirculation occurs in the first bend, but flow reversal is observed in several flow conditions. In the outer bank section of the second bend a flow recirculation cell with a vertical axis is observed that is likely caused by the outer bank widening.

The overall average shear layer flapping period is 13 seconds and is rather constant between flow conditions. The overall shear layer displacement range is 60 mm, which is 6% of the channel width and 43% of the average flow depth. No significant temporal trends can be discovered. However, with very little certainty it can be stated that the horizontal displacement range shows a linear trend with flow depth and a doubling of the Froude number causes the horizontal displacement range to multiply by roughly 6 times.

Flow depth has an influence on the location of the shear layer, an increase in flow depth results in the downstream movement of the shear layer. The downstream shift of the shear layer in deeper flow can be correlated to the adaptation length. However the downstream shift of the shear layer between the different flow depths is much smaller than the adaptation length calculation suggests. It is therefore unlikely that the location of the separation point is directly influenced by the adaptation length of flow, there could however be an indirect link.

The flow in the outer bank widening is separated, but no clear shear layer can be observed. However the separation and reattachment points can be observed. The larger the flow depth the smaller the extent of the outer bank separated zone.

Froude number has an influence on the location of the downstream end of the shear layer. It bends towards the inner bank with an increase in Froude number. The location of the separation point does however not depend on the Froude number.

The **Reynolds number** has influence on the turbulence and the boundary layer thickness. So an increase in Reynolds number leads to an increase in the chance of flow separation, because of a thinner boundary layer and more turbulence. The location of the separation point does not depend on the Reynolds number. The Reynolds number increases with increasing **flow depth** and/or **Froude number**, so there is a complex interrelationship.

The existence of an outer bank cell cannot be confirmed. Only in the high Froude number conditions a significant increase in water level, due to the transverse water level tilt, near the start of the outer bank of the first bend can be observed. In all experimental flow conditions, except the intermediate depth high Froude condition, the flow velocity near the outer bend bank is lower. This may indicate the existence of an outer bank cell.

7 Acknowledgements

Foremost, I want to thank Maarten Kleinhans for the support and supervision during the complete process of data analysis and thesis writing. I have experienced the guidance as very encouraging and motivating. I want to thank Stuart McLelland, Daniel Parsons, Rob Thomas and Arjan Reesink for the support and supervision during my stay in Hull. Especially thanks to Arjan Reesink for the delicious espressos and for providing a place to sleep. The data that is analyzed in this report was made possible by the European Community's Sixth Framework Programme through the grant to the budget of the Integrated Infrastructure Initiative HYDRALAB III within the Transnational Access Activities, Contract no. 022441 (Blanckaert et al., 2012).

8 References

8.1 Papers

Andrle, R., (1994). Flow structure and development of circular meander pools. Geomorphology 9, (1994), 261-270

Balen, W. van, (2010). Large eddy flow simulation for the prediction of bank erosion and transport processes in river bends. Ph.D. dissertation. Delft University of Technology, Delft, Netherlands

Bagnold, R. A., U.S. Geol. Surv. Prof. Pap., 282-E (1960)

Blanckaert, K., Kleinhans, M. G., McLelland, S. J., Uijttewaal, W. S., Murphy, B. J., Kruijs, A., Parsons, D. R. & Chen, Q. (2012). Flow separation at the inner (convex) and outer (concave) banks of constant-width and widening open-channel bends. Earth Surface Processes and Landforms

Blanckaert, K., Schnauder, I., Sukhodolov, A., Balen, W. & Uijttewaal, W.S.J. (2009). Meandering: field experiment, laboratory experiments and numerical modelling. River, Coastal and Estuarine Morphodynamics (RCEM), Santa Fe, Argentina, September 21-25

Blanckaert, K., Glasson, L., Jagers, H.R.A. & Sloff, C.J. (2003). Quasi-3D simulation of flow in sharp open-channel bends with horizontal and developed bed topography. Proc. Int. Symp. Shallow Flows, Vol. I, 93-100, Techn. Univ. Delft, Delft, The Netherlands

Blanckaert, K. (2011). Hydrodynamic processes in sharp meander bends and their morphological implications. Journal of Geophysical Research, 116(F1), F01003

Blanckaert, K. & de Vriend, H. J. (2003). Nonlinear modeling of mean flow redistribution in curved open channels. Water resources research, 39(12), 1375

Blanckaert, K. & De Vriend, H. J. (2004). Secondary flow in sharp open-channel bends. Journal of Fluid Mechanics, 498(1), 353-380

Bridge, S. (1993). The interaction between channel geometry, water flow, sediment transport and deposition in braided rivers. Geological Society, London, Special Publications 1993, v.75; p13-71

Bridges, P. H. & Leeder, M. R. (1976). Sedimentary model for intertidal mudflat channels, with examples from the Solway Firth, Scotland. Sedimentology, 23(4), 533-552

Ferguson, R. I., Parsons, D. R., Lane, S. N. & Hardy, R. J. (2003). Flow in meander bends with recirculation at the inner bank. Water resources research., 39(11), 1322

Hickin, E. J., (1977.) Hydraulic factors controlling channel migration. In Davidson-Arnott, R. and Nickling, W. (Eds), Research in Fluvial Systems, Proceedings of the 5th Guelph Geomorphology Symposium. Geobooks, Norwich. pp. 59-72

Hodskinson, A. & Ferguson, R. I. (1998). Numerical modelling of separated flow in river bends: Model testing and experimental investigation of geometric controls on the extent of flow separation at the concave bank. Hydrological Processes, 12(8), 1323-1338

Kleinhans, M. G., Schuurman, F., Bakx, W. & Markies, H. (2009). Meandering channel dynamics in highly cohesive sediment on an intertidal mud flat in the Westerschelde estuary, the Netherlands. Geomorphology, 105(3), 261-276

Kleinhans, M. G., Blanckaert, K., McLelland, S. J., Uijttewaal, W. S. J., Murphy, B. J., van de Kruijs, A. & Parsons, D. R. (2010). Flow Separation in sharp meander bends. Proceedings of the HYDRALAB III Joint User Meeting, Hannover, February 2010

Leeder, M. R. & Bridges, P. H. (1975). Flow separation in meander bends.

Nanson, G.C. & Croke J.C. (1992). A genetic classification of floodplains. Elsevier Science Publishers B.V., Amsterdam, Geomorphology, 4, p459-486

Ottevanger, W., Uijttewaal, W. S. J. & Blanckaert, K. (2010). Validation of a non-linear reduced hydrodynamic model for curved open-channel flow.

Page, K. & Nanson, G. (1982). Concave-bank benches and associated floodplain formation, Earth Surface Processes Landforms, 7, 529-543

Rozovskii, I. L., (1957). Flow of Water in Bends of Open Channels. Academy of Sciences of the Ukrainian SSR, Israel Program for Scientific Translations, Jerusalem, 1961

Schlichting, H., & Gersten, K. (2000). Boundary-layer theory. Springer.

Smith, D. G., Hubbard, S. M., Leckie, D. A. & Fustic, M. (2009). Counter point bar deposits: lithofacies and reservoir significance in the meandering modern Peace River and ancient McMurray Formation, Alberta, Canada. Sedimentology, 56(6), 1655-1669

Smith, D. G. & Pearce, C. M. (2002). Ice jam-caused fluvial gullies and scour holes on northern river flood plains. Geomorphology, 42(1), 85-95.

Struiksma, N., Olesen, K., Flokstra, C. & De Vriend H. (1985). Bed deformation in curved alluvial channels. Journal of Hydraulic Research 23:57–79.

Van Dyke, M., An Album of Fluid Motion, Parabolic Press, 12th edition, 1982

Zeng, J., Constantinescu, G., Blanckaert, K., & Weber, L. (2008). Flow and bathymetry in sharp open-channel bends: Experiments and predictions. Water Resources Research, 44(9), W09401

8.2 Books

Anderson, John D. (2004), Introduction to Flight, McGraw-Hill

Clancy, L.J. (1975), Aerodynamics, Pitman Publishing Limited, London

8.3 Websites

Baes, J. (2012). Open Questions in Physics. <http://math.ucr.edu>, accessed 15 September 2013, last modified: July 2012

Franklin Institute (1999). Laminar, Turbulence, Transition and Flow Separation. Cislunar Aerospace. <http://www.fi.edu>, accessed 6 September 2013, last modified: 11 February 1999

Marx, D. (2010). Stream and Peaks of the Taylor Hilldegard Wilderness. <http://thelightroomlab.com>, accessed 15 September 2013, last modified: 8 December 2010

9 Appendices

9.1 Properties of the different conditions and settings used in FlowScout

0408f – gain=2– exposure=5ms

	Nr of images	Bend nr.	L wall (m)	R wall (m)	Search dist	Vector validation	PC
1	1961	1 ds		7.253 (M100)	35x35	-300,-500,50,50	B1
2	1563	1		6.55	30x30	-400,-400,50,50	A1

0520f – gain=2 – exposure=5ms

	Nr of images	Bend nr.	L wall (m)	R wall (m)	Search dist	Vector validation	PC
1	2000	1 ds		7.253 (M100)	15x15	-150,-225,80,80	B1
2	2496	1		6.90 and 6.55	18x18	-230,-260,80,80	A1

0620f – gain=2– exposure=***ms

	Nr of images	Bend nr.	L wall (m)	R wall (m)	Search dist	Vector validation	PC
01 5ms	1220	1		6.90 and 6.55	50x50	-750,-750,300,300	?
02 8ms	1434	1		6.90 and 6.55	50x50	-750,-750,300,300	?
03 8ms	2141	1 ds		7.253 (M100)	50x50	-750,-750,300,300	?

0708f – gain=2 – exposure=***ms

	Nr of images	Bend nr.	L wall (m)	R wall (m)	Search dist	Vector validation	PC
01 8ms	1573	2 ds		12.715 (B280)	30x30	-450,-400,150,150	A3
02 5ms	2508	2 R wall		10.705 (B245)	30x30	-400,-400,100,100	A4
03 8ms	1448	2 L wall		8.253 (B200)	35x35	-350,-600,50,50	A5
04 8ms	2023	2 us R wall		9.36	35x35	-250,-500,50,50	A6

0820f – gain=2 – exposure=8ms

	Nr of images	Bend nr.	L wall (m)	R wall (m)	Search dist	Vector validation	PC
1	2121	2 us R wall		9.355	20x20	-200,-250,80,80	A3
2	2272	2 us L wall	9.790 (B200)		20x20	-200,-250,80,80	A4
3	2517	2 apex R wall		10.705	15x15	-200,-200,80,80	A5
4	2596	2 ds	10.80		15x15	-220,-150,80,80	A6

0920f – gain=2 – exposure=8ms

	Nr of images	Bend nr.	L wall (m)	R wall (m)	Search dist	Vector validation	PC
1	2552	2 ds R wall	10.80		40x40	-600,-600,150,150	A3
2	3013	2 apex R wall		10.705	40x40	-600,-600,250,250	A4
3	1991	2 us R wall		9.36	60x60	-700,-900,250,250	A5
4	1618	2 apex L wall		8.253 (B200)	60x60	-700,-900,150,150	A6

1314f – gain=2 – exposure=8ms

	Nr of images	Bend nr.	L wall (m)	R wall (m)	Search dist	Vector validation	PC
1	2859	2 R wall		9.322	50x50	-750,-750,150,150	B1
2	2283	2 L wall	9.862		50x50	-500,-750,150,150	A6
3	3110	2 ds R wall	10.890		40x40	-750,-350,150,150	A4
4	3788	2 apex R wall		10.705	40x40	-750,-350,200,200	A1
5	2377	1 ds middle		7.253	50x50	-250,-750,200,200	A5
6	2701	1		6.564	50x50	-750,-750,200,200	A3

1414f – gain=2 – exposure=8ms

	Nr of images	Bend nr.	L wall (m)	R wall (m)	Search dist	Vector validation	PC
1	2497	2 ds L wall	9.862		15x15	-240,-240,20,20	A5
2	2605	2 us R wall		9.322	17x17	-250,-250,40,40	A6
3	3741	2 apex R wall		10.705	13x13	-190,-160,60,60	B1
4	3322	2 ds R wall	10.890		13x13	-190,-160,60,60	A3
5	3175	1 ds		7.253	16x16	-190,-220,60,60	A6
6	2932	1		6.564	15x15	-210,-230,60,60	A5

1508f – gain=2 – exposure=8ms

	Nr of images	Bend nr.	L wall (m)	R wall (m)	Search dist	Vector validation	PC
1	2543	1		6.572	13x13	-180,-180,35,35	A6
2	3173	1 ds		7.253	13x13	-130,-170,35,35	A5
3	2579	2 us R wall		9.910	13x13	-120,-180,15,15	A3
4	2474	2 L wall	9.79 (B200)		15x15	-130,-200,15,15	A4
5	3343	2 R wall		10.705(B245)	13x13	-140,-170,50,50	A1
6	3044	2 ds R wall	10.858		13x13	-160,-160,50,50	B1

9.2 Surface flow structure first bend [ms^{-1}]

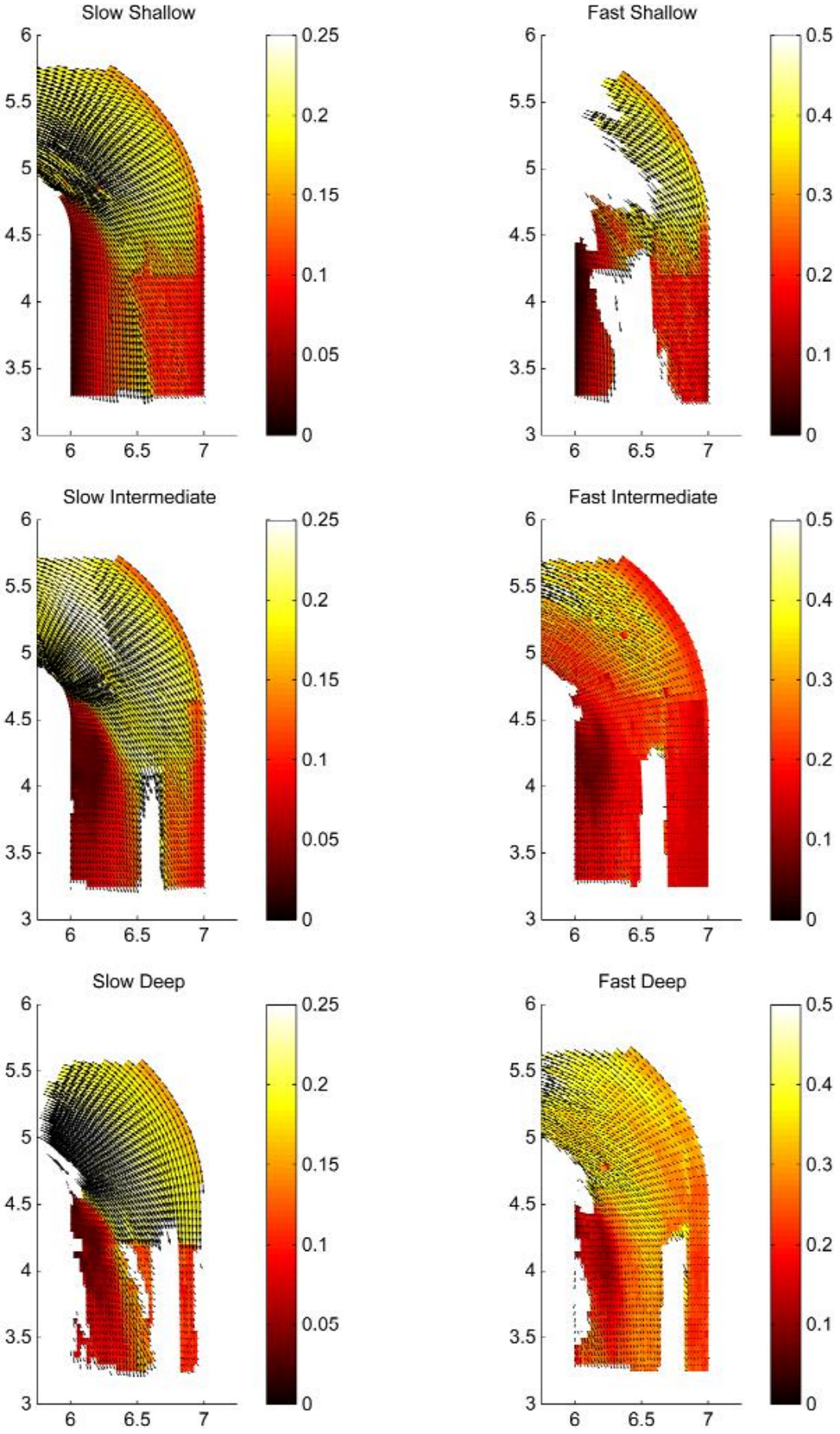

9.3 Surface flow structure separated zone, first bend [ms^{-1}]

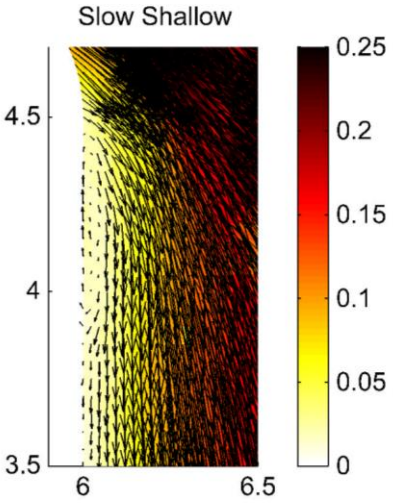

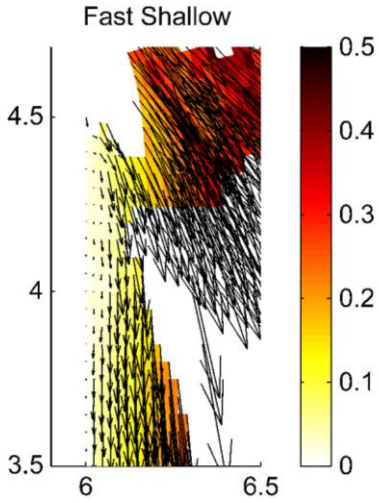

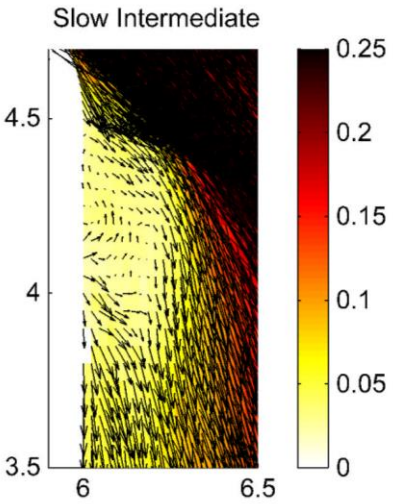

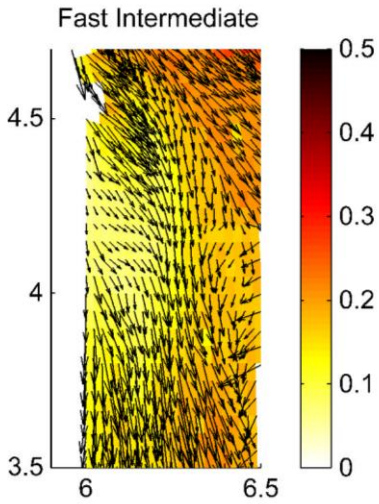

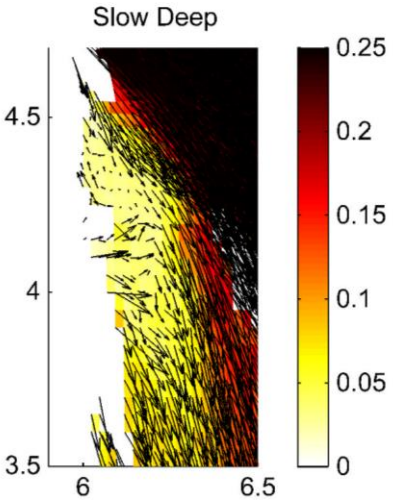

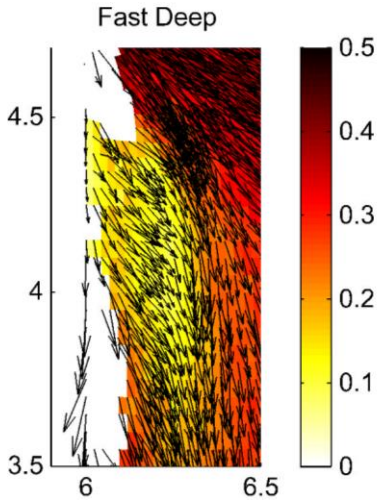

9.4 Surface flow structure second bend [ms^{-1}]

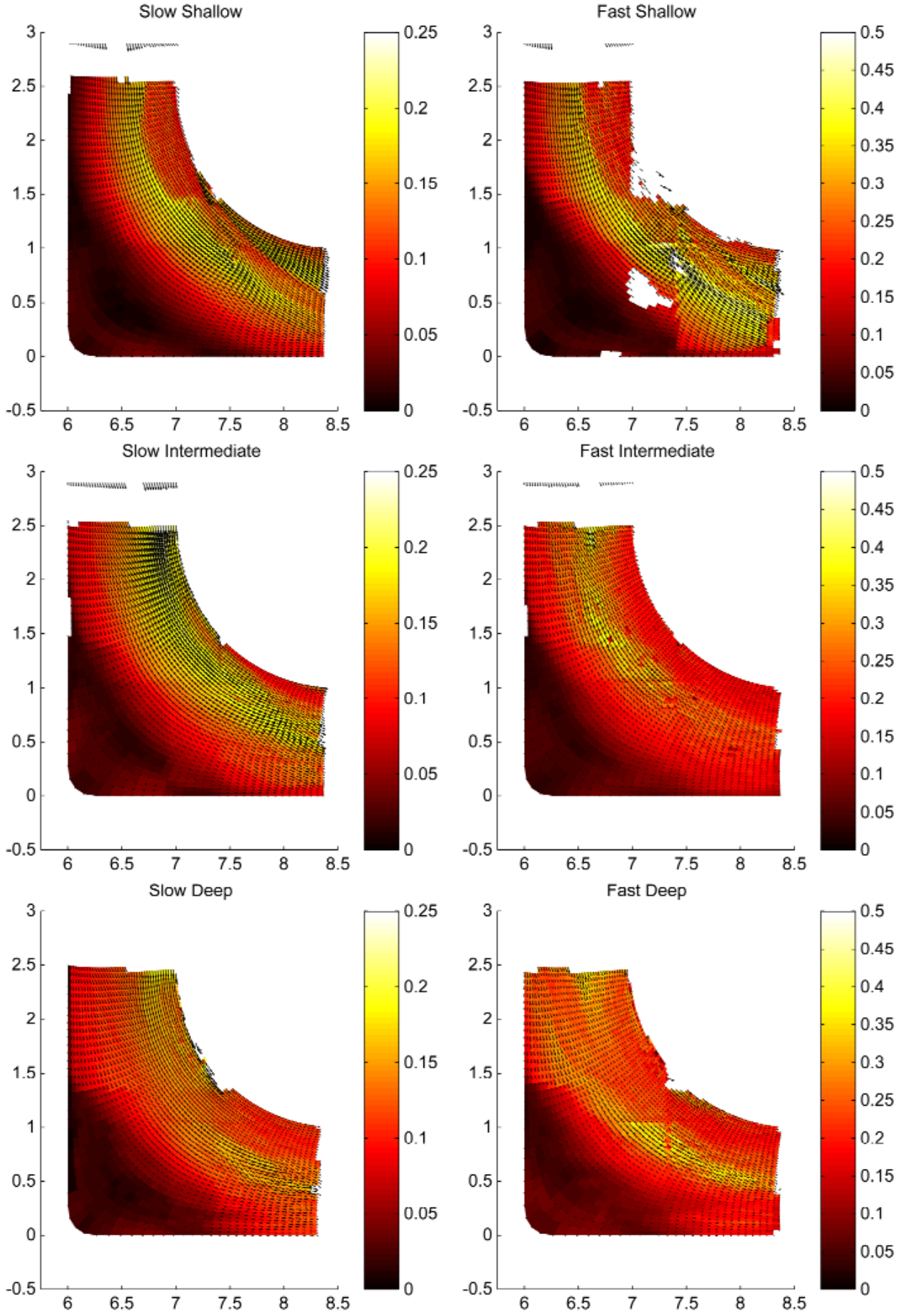

9.5 Surface flow structure separated zone, second bend [ms^{-1}]

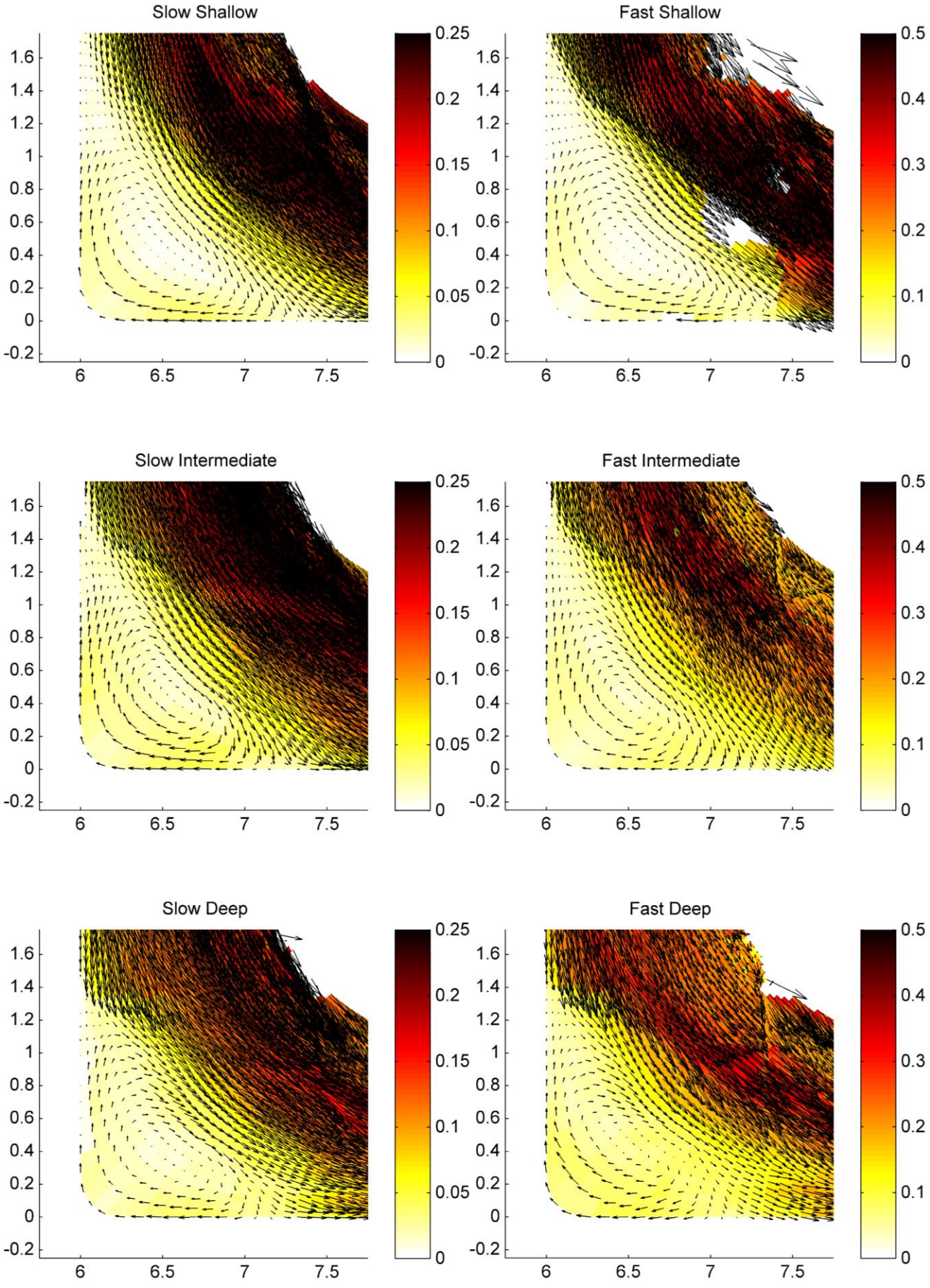

9.6 Vorticity first bend [s^{-1}]

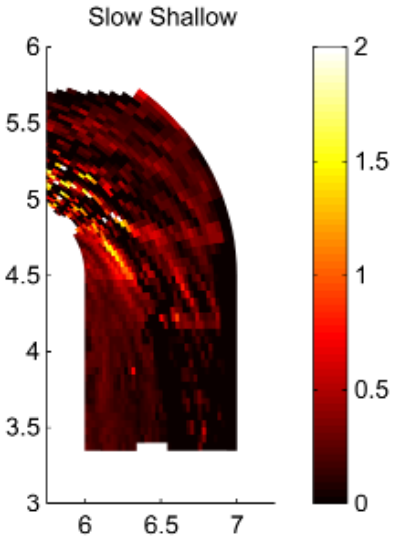

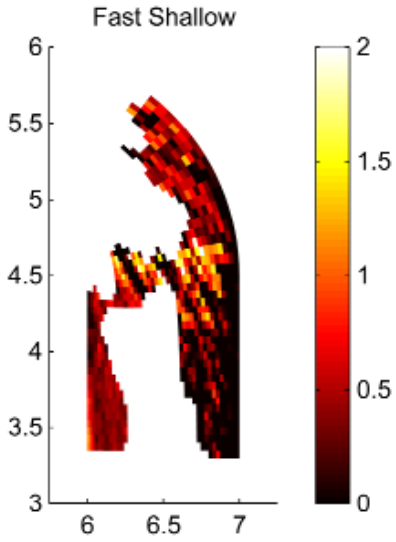

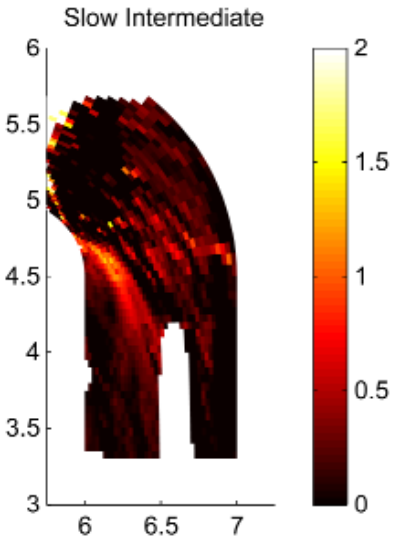

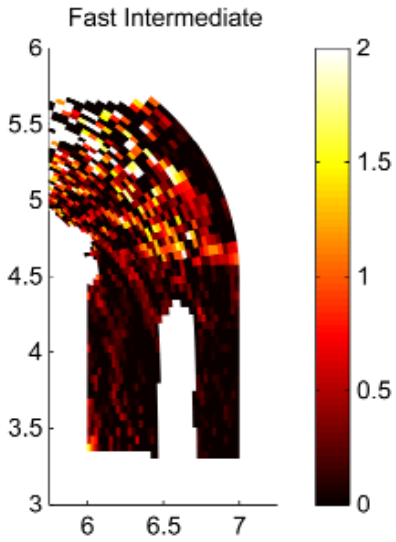

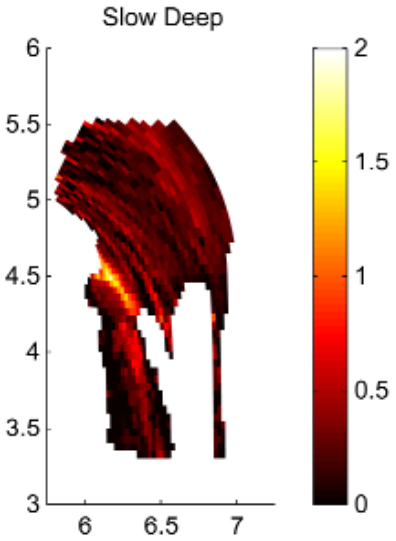

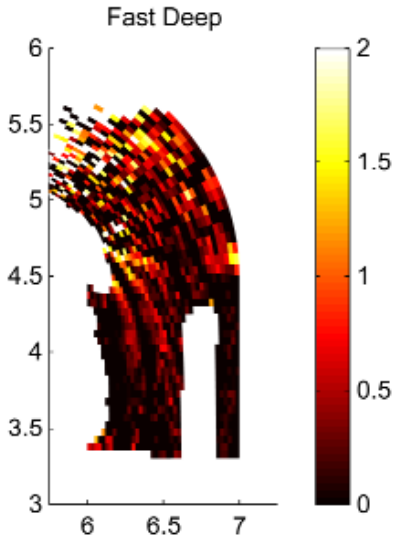

9.7 Vorticity second bend [s^{-1}]

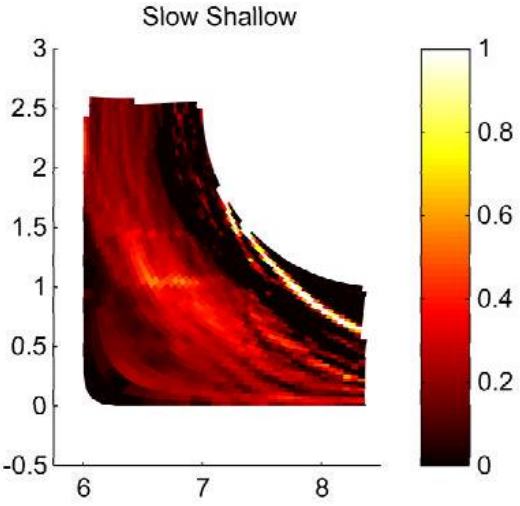

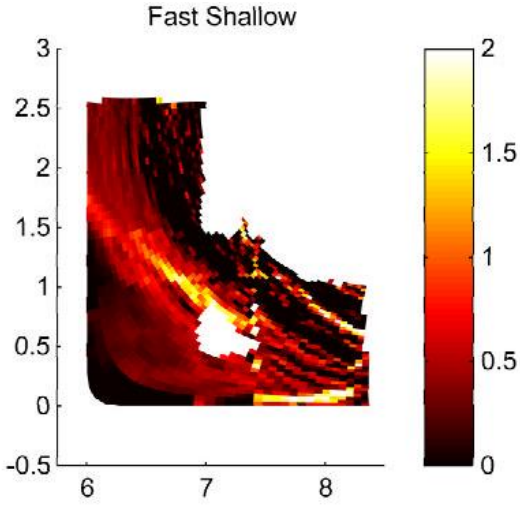

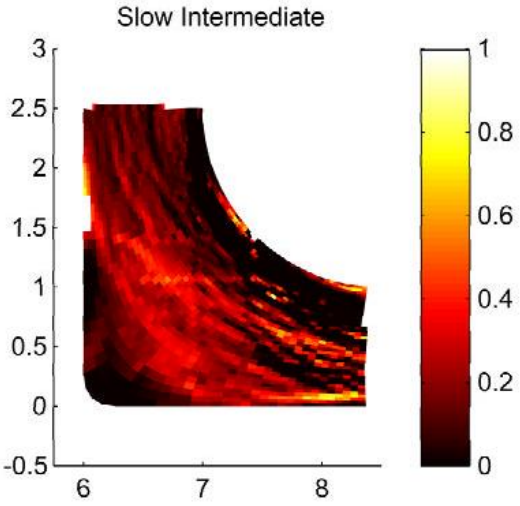

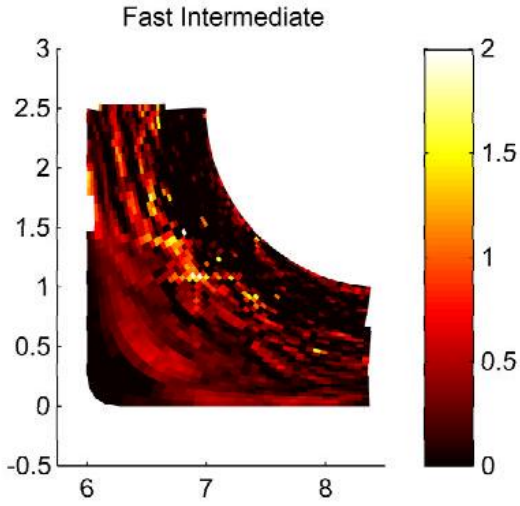

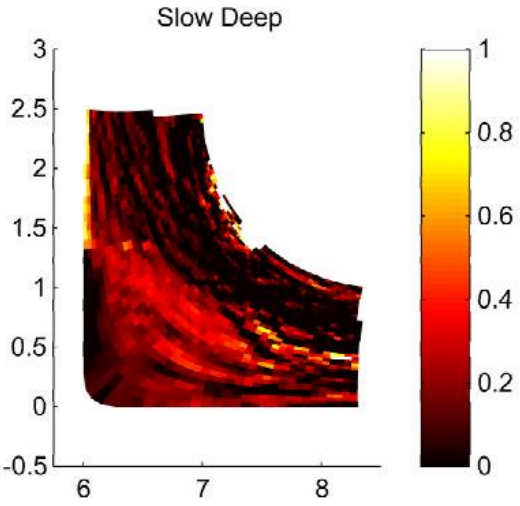

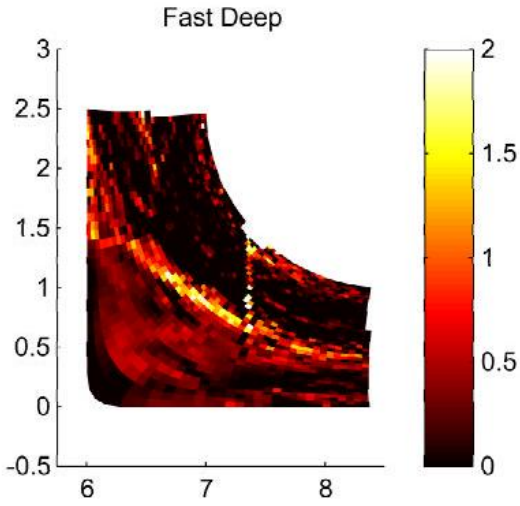

9.8 Time Stack plots

9.8.1 Shallow Slow

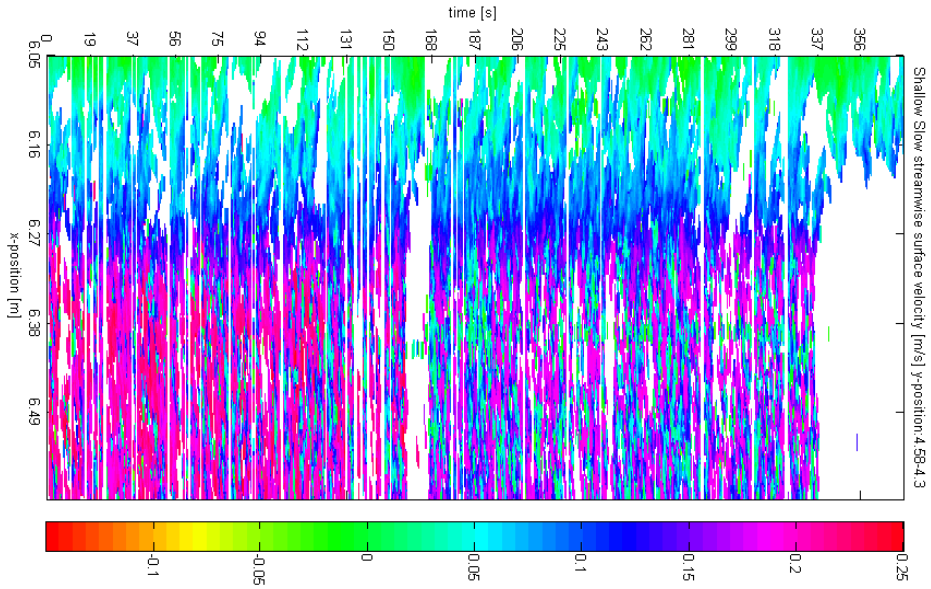

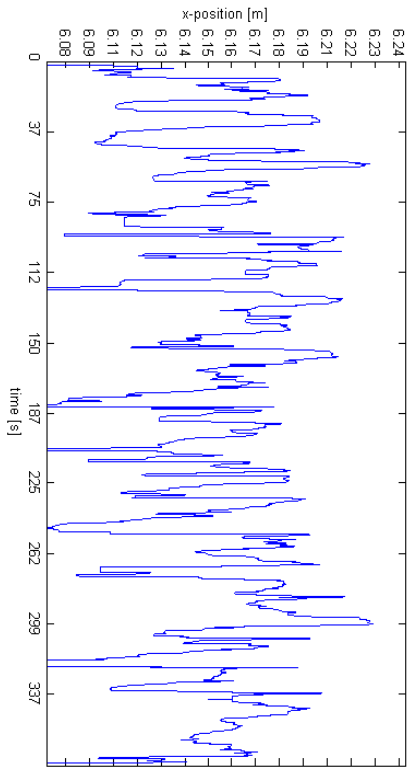

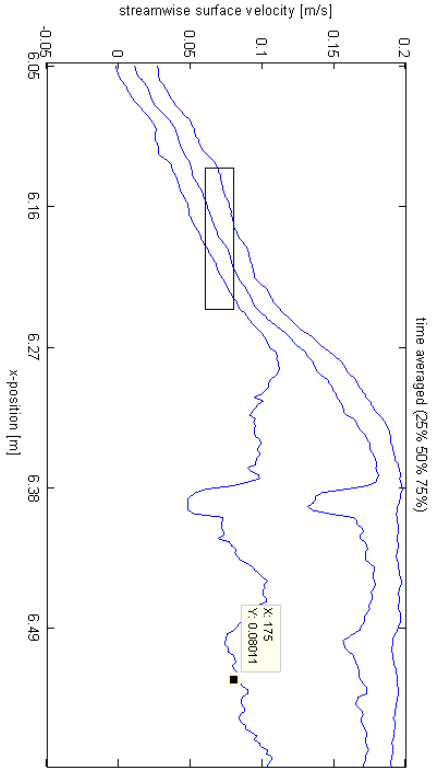

9.8.2 Shallow Fast

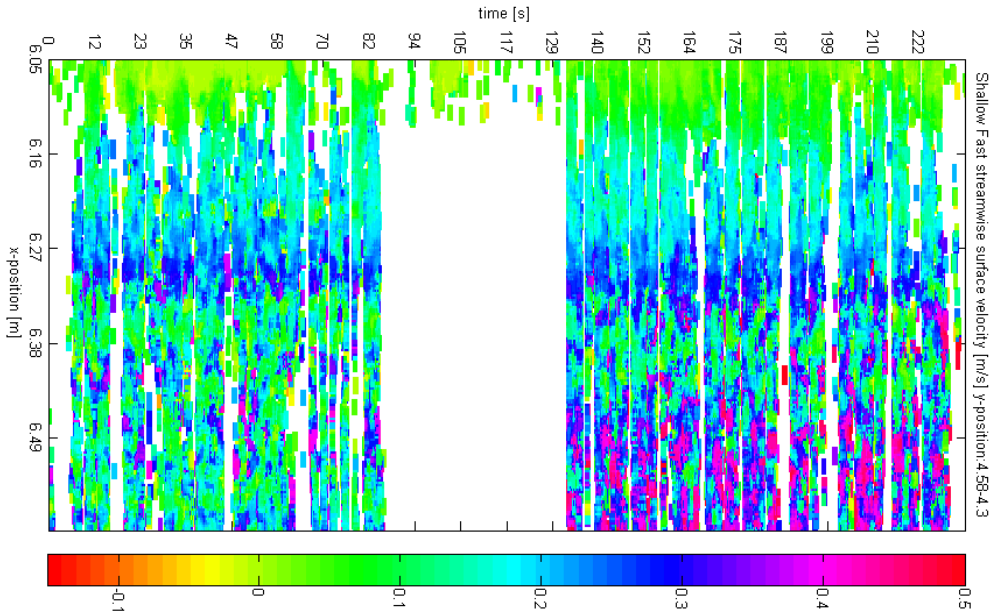

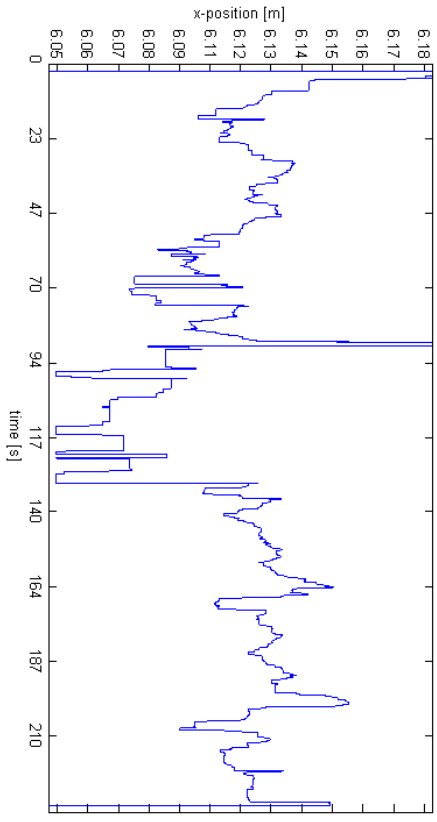

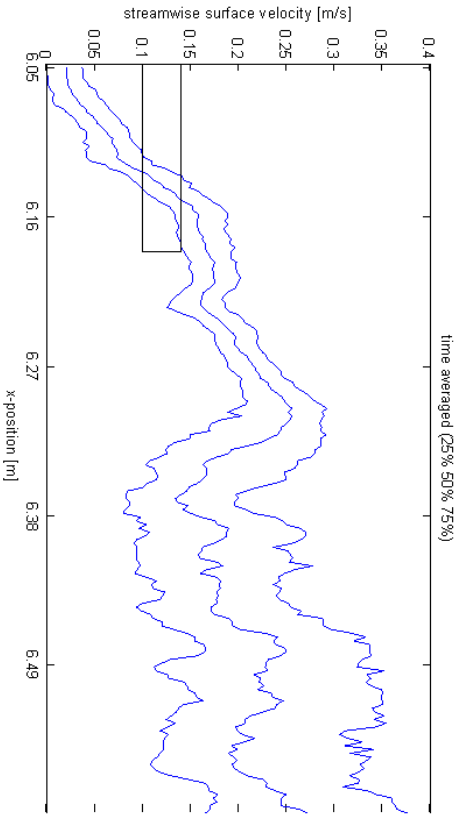

9.8.3 Intermediate Slow

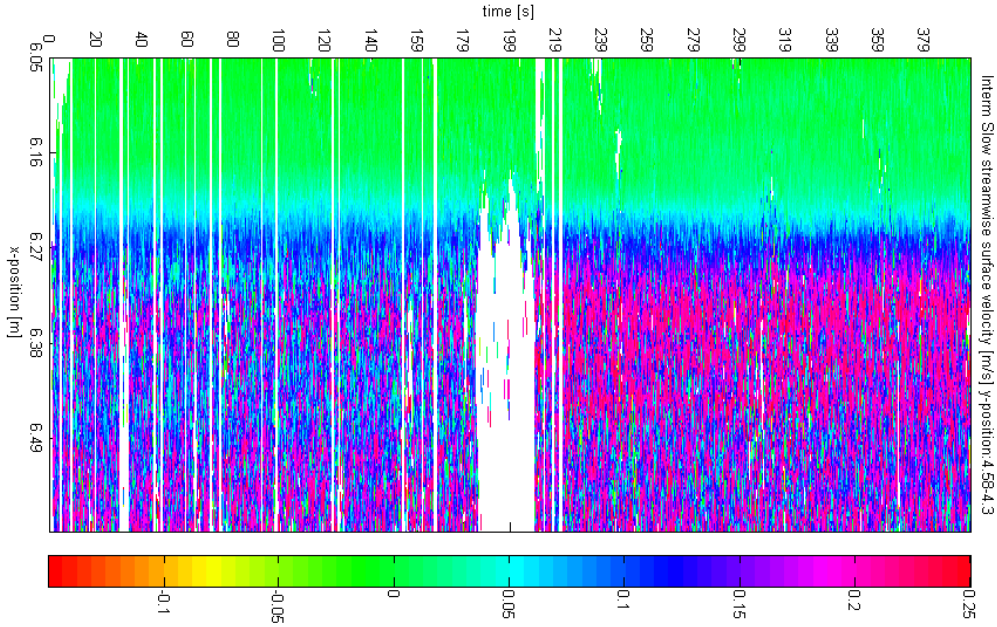

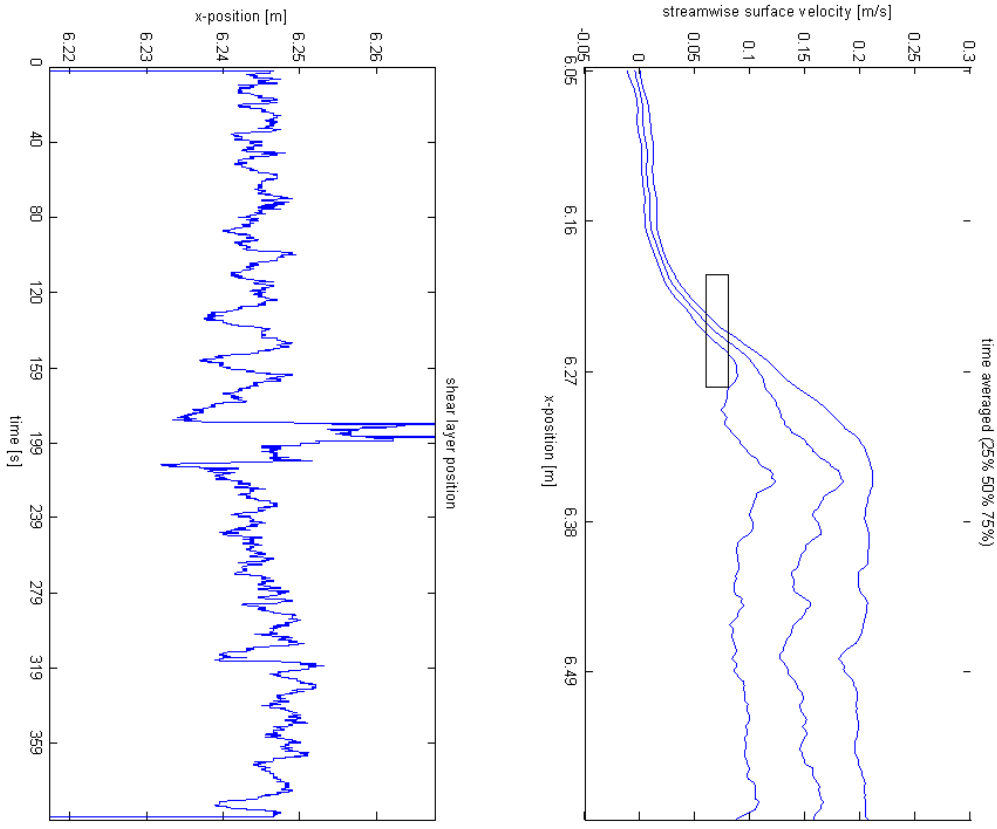

9.8.4 Intermediate Fast

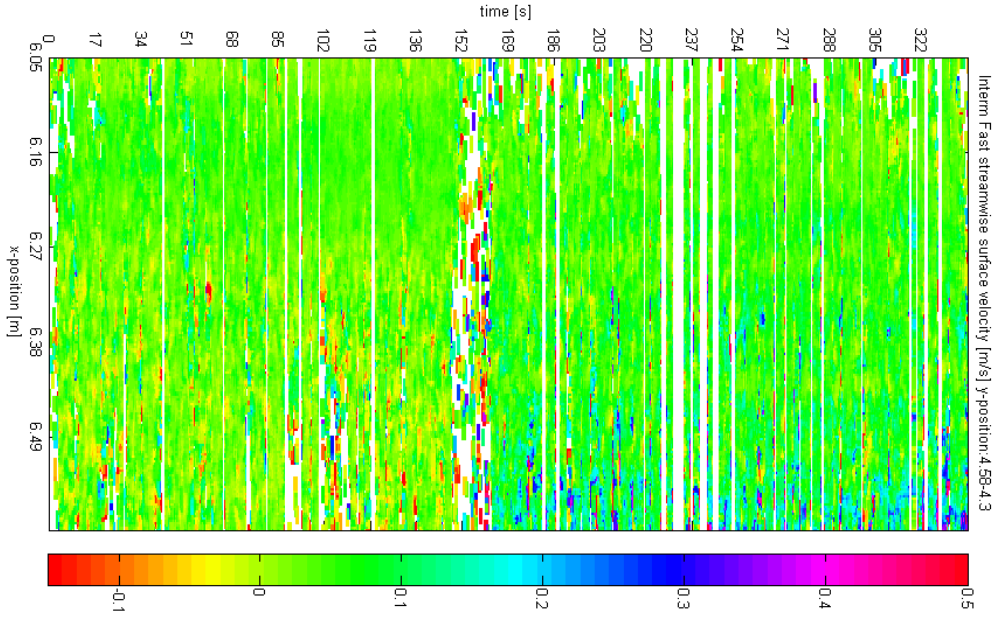

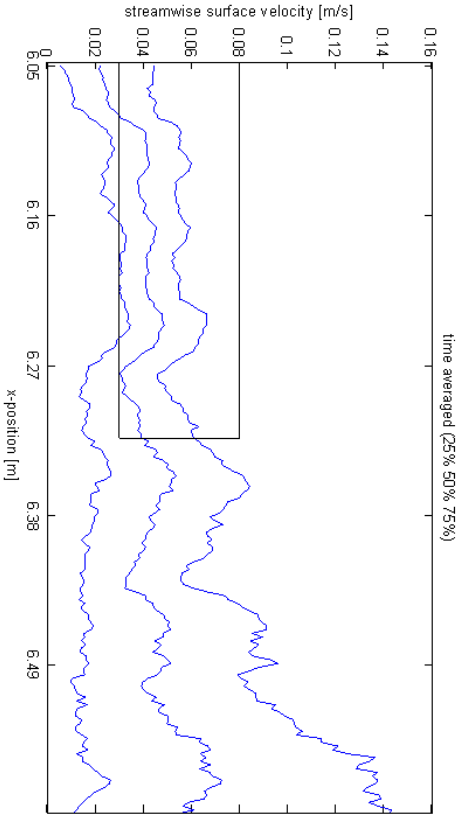

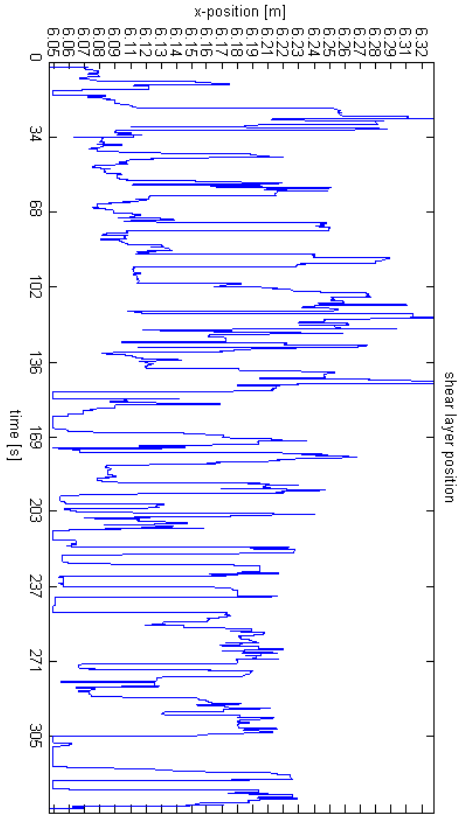

9.8.5 Deep Slow

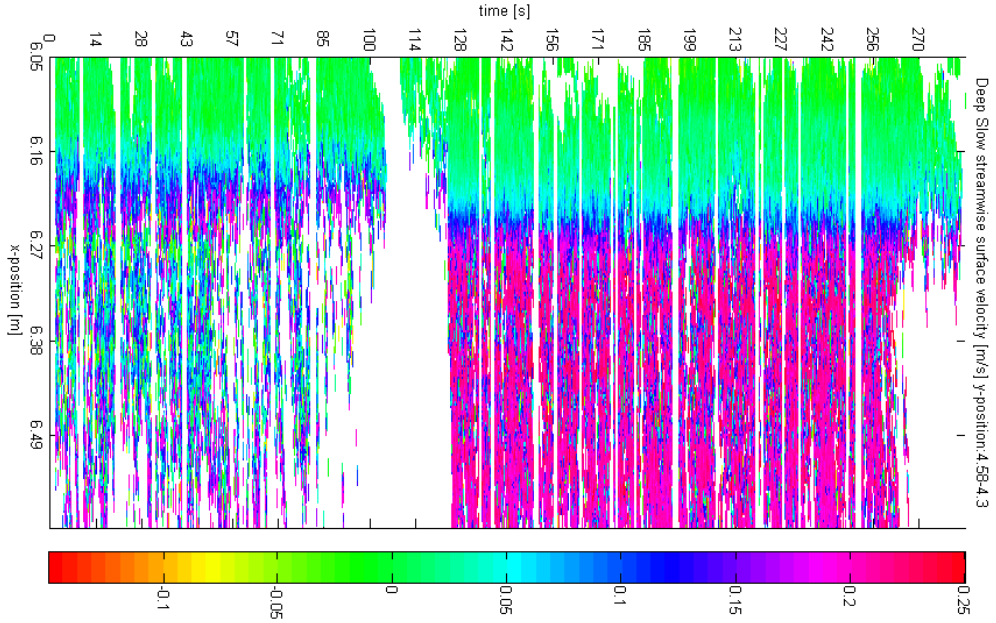

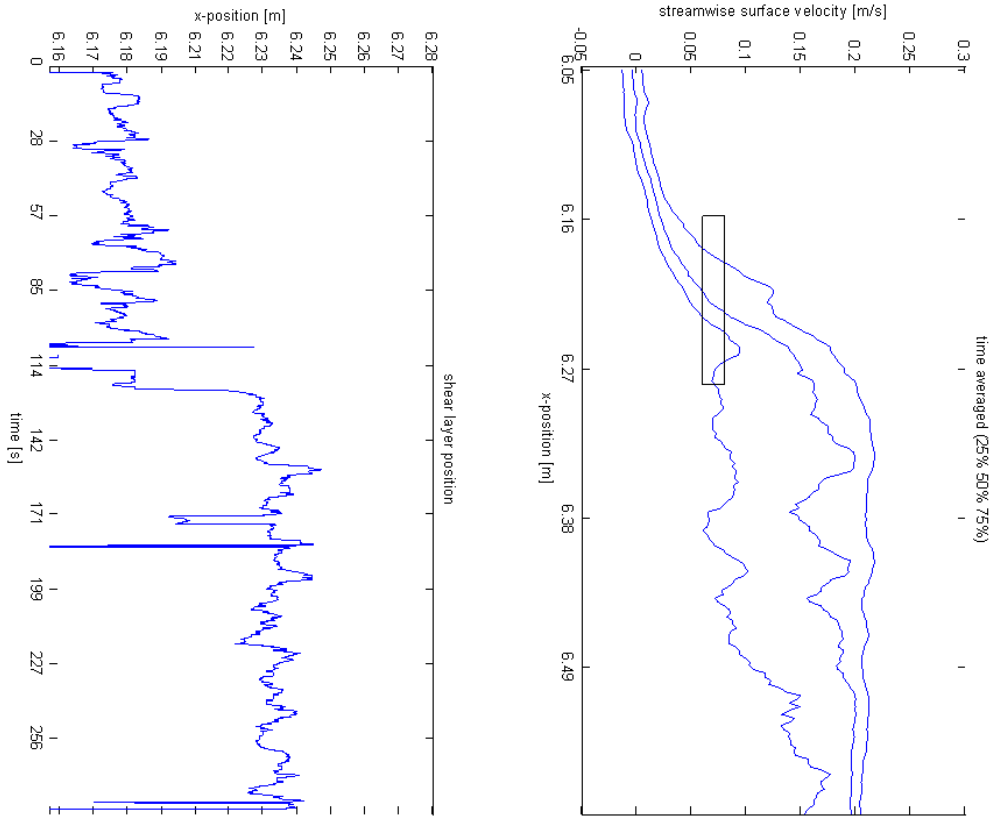

9.8.6 Deep Fast